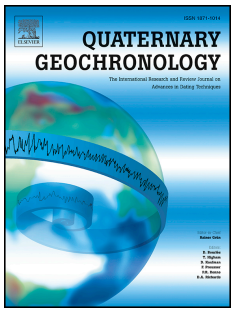

An (U-Th)/He age for the small Monturaqui impact structure, Chile

Ingrid Ukstins, Jo-Anne Wartho, Nathalie A. Cabrol, Edmond A. Grin, Matthijs C. van Soest, Marc B. Biren, Kip V. Hodges, Guillermo Chong

PII: S1871-1014(21)00067-4

DOI: https://doi.org/10.1016/j.quageo.2021.101217

Reference: QUAGEO 101217

To appear in: *Quaternary Geochronology*

Received Date: 4 February 2021

Revised Date: 23 July 2021

Accepted Date: 28 July 2021

Please cite this article as: Ukstins, I., Wartho, J.-A., Cabrol, N.A., Grin, E.A., van Soest, M.C., Biren, M.B., Hodges, K.V., Chong, G., An (U-Th)/He age for the small Monturaqui impact structure, Chile, *Quaternary Geochronology* (2021), doi: https://doi.org/10.1016/j.quageo.2021.101217.

An (U-Th)/He age for the small Monturaqui impact structure, Chile.

Ingrid Ukstins (1*), Jo-Anne Wartho (2,3), Nathalie A. Cabrol (4,5), Edmond A. Grin (4,5), Matthijs C. van Soest (2), Marc B. Biren (2), Kip V. Hodges (2) and Guillermo Chong (6)

(1) School of Environment, The University of Auckland, Private Bag 92019, Auckland 1142, New Zealand. Ingrid.Ukstins@auckland.ac.nz

(2) School of Earth and Space Sciences, PO Box 871404, Arizona State University, Tempe, AZ 85287, USA.

(3) GEOMAR Helmholtz Centre for Ocean Research Kiel, Wischhofstr. 1-3, 24148 Kiel, Germany.

(4) NASA Ames Research Center, Moffett Field, CA 94035, USA.

(5) SETI Institute, Mountain View, CA 94043, USA.

(6) Departmento de Ciencias Geológicas, Universidad Católica del Norte, Antofagasta, Chile.

Abstract

Single-crystal (U-Th)/He dating of 32 apatite and zircon crystals from an impact breccia yielded a weighted mean age of 663 ± 28 ka (n = 3; 4.2% 2σ uncertainties) for the Monturaqui impact structure, Chile. This ~350 m diameter simple crater preserves a small volume of impactite consisting of polymict breccias that are dominated by reworked target rock clasts. The small size, young age and limited availability of melt material for traditional geochronological techniques made Monturaqui a good test to define the lower limits of the (U-Th)/He system to successfully date impact events. Numerical modelling of ^{4}He loss in apatite and zircon crystals shows that, for even small craters such as Monturaqui, the short-lived compressional stage and shock metamorphic stage can account for the observed partial to full resetting of (U-Th)/He ages in accessory minerals. Despite the distinctly different ^{4}He diffusion parameters of apatite and zircon, the 2σ-overlapping youngest ages are recorded in both populations of minerals, which supports the inference that the weighted mean of the youngest (U-Th)/He population is the age of formation of this impact structure.

Introduction

Bolide impacts represent instantaneous events on geological timescales, and geochronological dating of crater formation should produce precise and accurate ages. However, most isotopic dating systems are not completely reset by impact processes. As little as ~10% of the target rocks affected by an impact event record impact-generated ages (Bogard et al., 1988; Schärer and Deutsch, 1990), which results in ambiguity when dating whole rock samples or mineral separates (Deutsch and Schärer, 1994). Of the 200 currently known terrestrial impact structures (excluding 4 historical events), 45% have been geochronologically analyzed, but only 21 % yield ages with <5% 2σ uncertainties (Earth Impact Database, 2020; Schmieder and Kring, 2020). Typical geochronological dating of impact samples utilizes U-Pb, ^{40}Ar-^{39}Ar, K-Ar, ^{14}C, fission track, ^{10}Be, ^{26}Al, U-Th series, paleomagnetic, thermoluminescence, and optically-stimulated luminescence techniques (Schmieder and Kring, 2020 and references therein).

The amount of melt produced at impact structures scales up with crater dimensions, and the proportion of target rock clasts in impact melt material decreases with the volume of melt produced (Grieve and Cintala, 1977). Large impact sites are more straightforward to date than small ones because melt products are both more abundant and less contaminated with unmelted xenocrysts and xenoliths, thus dating of these materials often yields valid reset ages using traditional geochronological methods such as U-Pb and ^{40}Ar-^{39}Ar (e.g., Hodych and Dunning, 1992; Kelley and Gurov, 2002). Nearly all (98%) of the crater ages with >5% 2σ precision comes from impact structures with diameters of ~5-250 km (Earth Impact Database, 2020; Schmieder and Kring, 2020). However, 86% of know impact craters on Earth are medium- to small-sized (simple to complex central-uplift-peak craters up to 30 km in diameter), and 26% of all craters have diameters of <3 km (Earth Impact Database, 2020; Schmieder and Kring, 2020).

Because of the small volume of melt produced from <3 km craters, traditional geochronological techniques that rely on impact melt or neoblastic minerals from crystallized impact melts are not tractable. Therefore, dating of these small impact structures instead relies on methods such as ^{14}C, cosmogenic nuclides, luminescence and paleomagnetic techniques, which often have age range limitations or low precision (e.g., Veski et al., 2004; Salminen et al., 2006; Nakamura et al., 2014; Sighinolfi et al., 2015). Of the forty-nine <3 km diameter terrestrial craters (excluding 4 historical craters), only one impact structure has an age with a 2σ precision of <5%; the 7.315 ± 0.080 ka Macha Field craters (1.1% 1σ; ^{14}C charcoal; Gurov and Gurova, 1998).

More recently, the (U-Th)/He thermochronological method has been successfully applied to both melt materials and unmelted impact breccias from impact structures. The technique relies on the resetting of ^{4}He in U- and Th-bearing minerals, and has been successfully applied to apatite, titanite and zircon from multiple impact structures (van Soest et al., 2011; Wartho et al., 2012; Young et al., 2013; Wielicki et al. 2014; Biren et al., 2014, 2016, 2019). While a single-crystal (U-Th)/He analysis generally has lower precision (~6-10% and sometimes up to 30% 2σ uncertainties) compared to typical ^{40}Ar-^{39}Ar and U-Pb analyses, multiple replicate (U-Th)/He analyses can be very accurate (Hourigan et al., 2005) and have resulted in robust impact formation ages. (U-Th)/He studies of minerals from impact structures include: (i) impact melt rocks from Manicouagan, Haughton and Clearwater East and West (van Soest et al., 2011; Young et al., 2013; Biren et al., 2016); (ii) lightly shocked (5-15 GPa) impact breccias from Wetumpka (Wartho et al., 2012); (iii) rapidly exhumed and cooled rocks from the Manicouagan central uplift peak (Biren et al., 2014); (iv) shocked and brecciated impactites from Morokweng (Wielicki et al., 2014); and (5) impact melt ejecta from an Ocean Drilling Program drill core sample, located ~390 km from the Chesapeake Bay impact structure (Biren et al., 2019).

This Monturaqui study utilizes the (U-Th)/He technique to date single apatite and zircon grains in two impactite breccia samples, containing clasts of local target rocks, from the small (350 m diameter) Chilean impact crater. In addition, ^{4}He diffusion modeling of apatite and zircon grains during (i) impact compression and (ii) adiabatic decompression with associated shock metamorphism, illustrate the effects of these thermal processes in fully or partially resetting (U-Th)/He ages, even in very small (<1 km) diameter craters.

Background

The Monturaqui impact crater is located at the southern end of Salar de Atacama in the Precordillera of northern Chile (3015 m elevation; 23° 55’ 39.28” S, 68° 15’ 41.63” W). It is the second smallest crater in South America, and existing ^{26}Al, ^{36}Cl and thermoluminescence ages suggest that it is the oldest of the 25 smallest craters on Earth (Schmieder and Kring, 2020). Monturaqui is a well-preserved, simple crater that formed in a Paleozoic basement granite (441 ± 8 Ma; 2σ; Rb-Sr whole rock; Mpodozis et al., 1983) containing zircons and apatites (Bunch and Cassidy, 1972), which is cut by 1-2 m wide mafic dikes and is overlain by a thin (~5 m) sheet of Pliocene Tucucaro ignimbrite (3.2 ± 0.3 Ma; K-Ar whole rock; Ramirez and Gardeweg, 1982; Fig. 1). The crater has a sub-circular morphology with a preferential NW-SE elongation (370 m E-W, 350 m N-S, and 34 m deep; Ugalde et al., 2007). Both granite and ignimbrite are exposed in the walls of the crater, but the rim crest is dominantly draped by ignimbrite outcrop. It was first proposed as an impact structure in 1966 based on the presence of iron shale, inferred to be altered fragments of the Fe-Ni impactor. The impactites are described as “porous cindery aggregates containing fragments of granite and bonded with glass", which are preferentially deposited on the southern and southeastern crater flanks (Sanchez and Cassidy, 1966;

Kloberdanz, 2010; Ukstins Peate et al. 2010; Rathbun et al. 2017). The impactor is postulated to be a Group I coarse octahedrite iron meteorite based on the composition of Fe-Ni spherules found in the impactite breccias and the structure of iron shale fragments (Sanchez and Cassidy, 1966; Buchwald, 1975).

Initial studies on the Monturaqui impact structure assigned an age of Pleistocene to Recent, based on the apparent disruption of the local Pleistocene drainage patterns (Sanchez and Cassidy, 1966). Thermoluminescence analysis of quartz grains extracted from an impactite produced an age estimate of 590 ± 60 ka (1σ; Verdugo and Cartes, 2000). Valenzuela et al. (2009) used cosmogenic radionuclide dating techniques on quartz mineral separates from granite outcrops within the crater and residual activities of iron shale samples, to both evaluate the age of the crater and to obtain ages of the fragmented impactor. Age data from the granite produced concordant results for ^{10}Be with an age range of 200 to 250 ka, but this is likely to be a minimum age due to subsequent erosion of the crater walls. The iron shale produced ^{36}Cl and ^{26}Al ages of 500-600 ka, and paleomagnetic analyses suggested a granite remagnetization age of 780 ka, therefore the Monturaqui impact age was estimated to be between 500-780 ka (Valenzuela et al., 2009).

Description of samples and electron microprobe imaging and analyses

The impactite breccia samples were described by Bundy and Cassidy (1972) as cindery, highly vesicular agglomerations of shocked and unshocked granite fragments (several microns to 4 cm in size) and nickel-iron and sulphide spherules tightly bound in a highly heterogeneous glass matrix. The impactites have a twisted, ropy appearance, similar to volcanic bombs, which was probably caused by distortion during flight when most of the components were still hot. In

addition, the outer surfaces of the impactites have embedded ignimbrite pebbles, which are common on the terrain surfaces, suggesting that the impactites were still very hot and viscous when they struck the ground. The 441 ± 8 Ma Rb-Sr (Mpodozis et al., 1983) granite country rock is hypidiomorphic-granular in texture, consisting of zoned antiperthitic oligoclase-andesine, quartz, microcline, chlorite, biotite, magnetite (some grains with exsolved ilmenite), apatite, and zircon, as well as sericite and other alteration minerals (Bundy and Cassidy, 1972). The apatite and zircon grains (U-Th)/He dated in this study were most likely sourced from the granitic target rocks, rather than the welded dacitic ignimbrite, due to abundance.

Four zircon grains and fragments from each of two samples (CIUP 08099 and 08100) were photographed using a Leica MZ16 binocular microscope (Figs. 2-3). The grains were mounted on double-sided copper tape, carbon coated, and imaged and analysed using secondary electron (SE) and energy-dispersive spectrometry (EDS) on a JEOL JXA-8530F Hyperprobe field-emission electron microprobe, located at the John M. Cowley Center for High Resolution Electron Microscopy, ASU (Figs. 2-3). Operating conditions were 10 kV, a working distance of 11 mm, and for the EDS analyses a current of 305 pA was used, with a counting time of 20 seconds. Please note that it is not possible to undertake SE imaging and EDS analysis of the (U-Th)/He dated zircon and apatite grains, and hence only binocular microscope photomicrographs were obtained for the (U-Th)/He dated apatites and zircons (examples are shown in Fig. 4). The carbon coating plus sticky tape residue that is required for EMP analysis and SE imaging can cause extensive contamination of the noble gas extraction line and quadrupole mass spectrometer, resulting in interferences with the He isotopic measurements. For example, singly ionized deuterium (^{2}H) interferes with ^{4}He measurements, while ionized HD interferes with the ^{3}He spike isotopic measurements. Therefore, we only undertook SE imaging and EDS analysis

145 of non-dated zircon grains. Unfortunately, there were no remaining apatite grains or fragments
146 found in the two samples available for EDS analysis and SE imaging.
147
148 **Methods – (U-Th)/He dating**
149 We selected two impactite breccia samples from the Monturaqui crater, representing
150 different quadrants of the ejected material. Sample CIUP 08099 was collected from the south-
151 eastern flank of the crater, along the inferred impact trajectory, and CIUP 08100 originated from
152 the crater rim directly to the south (Fig. 1). Impactite fragments ranged in size from 2 mm to 3
153 cm, and a suite totalling 785 g and 840 g were selected for mineral separation from samples
154 CIUP 08099 and 08100, respectively. The samples were crushed, dry and wet sieved, and
155 magnetic separation and heavy liquid separation were used to generate apatite- and zircon-
156 bearing separates. Zircon and apatite grains were hand-picked for (U-Th)/He analysis on the
157 basis of their euhedral habit and apparent lack of inclusions. As many suitable apatites as
158 possible were selected from each sample as it was expected that apatite had the greatest chance
159 of recording the impact age due to its lower ^{4}He closure temperature (Farley, 2000) compared to
160 zircon (Reiners et al., 2004). A total of 10 zircon and 22 apatite grains were analyzed, 5 zircons
161 from each sample, plus 8 and 14 apatites from samples CIUP 08099 and CIUP 08100,
162 respectively.
163 The dimensions relevant for the application of the alpha ejection correction were
164 measured for each grain using photomicrographs taken at high magnification (184 x) with a
165 digital video camera attached to a Leica MZ16 binocular microscope (Fig. 4). The camera
166 images were calibrated to specific magnification stops on the microscope so that computer
167 software could be used to determine the relevant dimensions of the grains (Table 1).

Single grains were loaded into individual niobium (for zircon) and platinum (for apatite) microcrucibles, which were crimped to close and loaded into the sample holder of the Australian Scientific Instruments Alphachron at the Group 18 Laboratories at Arizona State University. The laser chamber was pumped down overnight and helium was extracted from each sample using a 45 W, 980 nm infra-red diode laser, using an energy output of approximately 10 W for apatite and 15 W for zircon. The ^{4}He gas was spiked with ^{3}He and cleaned of any reactive gases by exposure to a hot SAES NP-10 getter, before analysis on a Balzers Prisma QMS 200 quadrupole, equipped with Faraday and Channeltron electron multiplier detectors, which has a room temperature SAES NP-10 in the analysis chamber. All analyses were performed using the Channeltron electron multiplier. Between sample analyses, a known ^{4}He aliquot was spiked with ^{3}He and analyzed to allow the amount of unknown ^{4}He in the sample to be calculated. In addition to the samples, empty Nb and Pt tubes were analyzed as blanks, and several shards of Durango fluorapatite (32.0 ± 1.8 Ma; 2σ, n = 11) and grains of Fish Canyon zircon (27.7 ± 2.5 Ma (2σ; n = 5) were analyzed as age standards.

After ^{4}He analysis, the samples were unloaded from the laser chamber and dissolved for U and Th analysis. The apatites in their Pt capsules were loaded into 2 ml polypropylene vials and dissolved using 25 µl of 50 % nitric (HNO_3) acid that contained ~5 ng of ^{230}Th and ~15ng ^{235}U, which is used as a spike (Evans et al., 2005). The zircons require a more intense dissolution procedure, utilizing high temperature and pressure Parr digestion vessels, and concentrated hydrofluoric (HF), nitric (HNO_3), and hydrochloric (HCl) acids, which was modified slightly from the procedure described by Reiners (2005). After dissolution, samples, together with specially prepared batches of spiked standard solutions, were analyzed for ^{238}U and ^{232}Th concentrations on a ThermoElectron X-series inductively coupled plasma source mass

spectrometer in the W.M. Keck Foundation Laboratory for Environmental Biochemistry at ASU. Analytical errors were regularly between 1.0-2.6% (1σ) for both ^{238}U and ^{232}Th, but in some apatites the errors were significantly larger (up to 12%; 1σ; Table 1) due to the lower ^{238}U and ^{232}Th concentrations.

The ^{4}He, ^{238}U, and ^{232}Th data were then used to calculate raw dates using an iterative approach to solving the (U-Th)/He age equation as documented in Farley et al., (1996). Within this calculation, the concentration of ^{235}U is derived from the measured ^{238}U concentration using the known ratio of these isotopes in nature. The raw ages were then corrected for alpha ejection losses following the models of Farley et al. (1996) for apatite, and Hourigan et al. (2005) for zircon, assuming a homogeneous distribution of U and Th throughout the crystals. Analytical errors were propagated, but no errors were assigned to the values input into the alpha ejection correction calculation following standard protocols used in the (U-Th)/He dating community. (U-Th)/He dates for a single non-detrital sample are frequently overdispersed with regards to what would be expected from their analytical errors. This dispersion is assumed to be associated in part with the assumptions of the FT correction (ie. homogeneity of U-Th throughout the crystal, and perfect geometric shape) and can be quite dramatic especially for zircon, e.g., Hourigan et al. (2005), but for well-behaved samples, this is observed to be ~2-4% 2σ. The analyses yielded a total of 10 (from 10) successful zircon ages, and 12 (from 22) successful apatite ages. The lower success rate in the apatites may have been due to undetected mineral inclusions (n = 1; observed from subsequent high ^{4}He re-extraction values, indicating the presence of inclusions), low concentrations of U and Th (n = 0), or extremely low ^{4}He contents in many of the grains (n = 9; Table 1).

Methods – Modeling of ^{4}He diffusive loss via impact-related heating of apatite and zircon

Modelling of ^{4}He diffusive loss from minerals requires knowledge of the ^{4}He diffusion parameters, the sizes of the grains, and the temperatures and durations of the thermal events associated with the formation of an impact structure. We have determined durations and temperatures for each of the dominant impact-formation stages associated with the Monturaqui impact structure, and used the grain diameters from the (U-Th)/He analyses of the apatites and zircons.

During a bolide impact event, the short-lived initial contact and compressional stage (~0.0003-1 second for 0.35-250 km final crater diameters[1]) between the impactor and target rocks can generate temperatures in excess of 10,000 K near the impact point, with surrounding target rocks typically reaching temperatures of 500-3000°C (French 1998; Collins et al 2005). To calculate the duration of the initial compression stage for Monturaqui, we used the following equation:

$$\tau = d/Vi \qquad [1]$$

where τ is the duration of contact, d is the projectile diameter, and Vi is the impact velocity. In order to determine a Fe-Ni projectile diameter we used two online programs utilizing Pi-scaling, with the following parameters for the Monturaqui impact structure: final rim-to-rim crater diameter (350 m), transient crater diameter (224 m), impact velocity (18 km/s; Gillet and El Goresy, 2013), impact angle (45°), acceleration of gravity (9.8 m/s^2 for Earth), and target and projectile densities of 3.0 and 8.0 g/cm^3, respectively. The first online calculator used was *Crater* (Melosh and Beyer, 2002), which yielded a projectile diameter of 4.9 m and a total crater

[1] Calculated using the *Crater* software (Melosh and Beyer, 2002) and equation [1], with bolide diameters of 4.9 m and 9.3 km, an impact velocity of 18 km/s, an impact angle of 45°, and projectile and target densities ranging from 8.0-1.5 and 3.0-1.5 g/cm^3, respectively.

formation time of 2.4 seconds. The second online impact crater calculator used was *Impact and Explosion Effects*, version 4.02 (Holsapple, 2020). Using the same parameters listed above, a projectile diameter of 7.8 m and a total crater formation time of 2.3 seconds was determined. The estimated energy from the impact crater formation was calculated to range from 8 x 10^{13} to 2 x 10^{14} J (19-38 kt TNT).

Compared to the short-duration initial contact and compression stage, the subsequent adiabatic decompression associated with shock metamorphism affects target rocks for longer durations (milliseconds to minutes) with temperatures ranging from ~900-2500°C and up to 5,000°C (Walton et al., 2006; Schwenzer et al. 2008; Stöffler et al., 2018). Dynamic crystallization experiments in meteorites produced shock-melt pockets and shock veins and yielded shock metamorphism durations in the range of 8-17 minutes (Walton et al., 2006; Schwenzer et al., 2008), to shorter durations of 1.75 minutes to 1.2 seconds (Shaw and Walton, 2013), with an estimated minimum duration of ~0.2 seconds (Beck et al., 2007). As the total formation time of the Monturaqui impact structure is determined to be 2.3-2.4 seconds, we have modelled the shock metamorphism stage in apatite and zircon grains using maximum and minimum durations of 1 and 0.1 seconds, respectively (Table 2).

Shock metamorphism at Monturaqui is estimated to range from <10 GPa up to very high shock pressures of 65 GPa (Bunch and Cassidy, 1972), which can result in post-shock temperatures of ~1500-1700°C (Stöffler et al., 2018). As no decomposition or melting was observed in the apatite and zircon grains from Monturaqui, both compression and shock metamorphism temperatures of 1500 and 1600°C were used in the modeling. A maximum temperature of 1600°C was estimated as this is just below the apatite melting temperature (1608-

256 1670°C; Bhatnagor, 1969) and it is also lower than the decomposition temperature of zircon
257 (1690°C; Finch and Hanchar, 2003).

258 Post-impact hydrothermal processes can affect target rocks with temperatures of ~100-
259 400°C, and can last for thousands to millions of years in medium to large impact structures
260 (Newsom et al., 1986; Parnell et al., 2005; Rasmussen et al., 2019; Kring et al., 2020). However,
261 due to the small size of the Monturaqui impact crater and the lack of information on post-impact
262 hydrothermal temperatures and durations in such small craters, no ^{4}He loss modelling was
263 performed on this impact crater stage.

264 Therefore, modeling of ^{4}He losses were undertaken for apatites and zircons for the initial
265 contact and compression stage using durations of 0.00027 and 0.00043 seconds, temperatures of
266 1500 and 1600°C, apatite grain radii of 27.4, 52.9 and 32.9 µm (minimum, maximum and the
267 average of the 2 reset grains; Table 1), and zircon grain radii of 24.8, 40.6, and 40.6 µm
268 (minimum, maximum and the radii of the single reset zircon grain; Table 1). Longer durations of
269 0.1 and 1.0 seconds were used for the shock metamorphism decompression stage, with
270 temperatures of 1500 and 1600°C. An author-written MathCAD version 14 program was used
271 (modified from Wartho et al., 2003), with the appropriate ^{4}He diffusion parameters and diffusion
272 geometries (cylinder for apatite and sphere for zircon; Farley, 2000; Reiners et al., 2004; Table
273 2) and the diffusion equations of Crank (1975) listed below.

274 The fractional loss of ^{4}He from a sphere (zircon) was calculated using the following
275 equation:

276 $$1 - \frac{6}{\pi^2}\sum_n \frac{1}{n^2} \exp\left(\frac{-Dn^2\pi^2 t}{a^2}\right) \quad [2]$$

where a is the grain radius (cm), t is time (seconds), and D is the activation energy calculated from the following equation: $D = D_o \exp\left(-\frac{E}{RT}\right)$, where D_o is the frequency factor (cm^2/s), E is the activation energy (cal/mol), and R is the gas constant (1.987 cal/mol).

The fractional loss of He from a cylinder (apatite) was calculated using the following equation:

$$1 - \sum_n \left(\frac{4}{a^2\,(\alpha_n)^2}\right) \exp(-D\,(\alpha_n)^2\,t) \qquad [3]$$

where the integer α_n is the root of $J_o(a\alpha_n) = 0$, and $J_o(x)$ is the Bessel function of first kind of order zero. Because diffusion is strongly affected by grain size, the modelling used the smallest, largest and average radii of the reset grains for the apatites and zircons (i.e., the R2 values in Table 1; Table 2).

Results: Optical and SE imaging, and EDS analyses

EDS analyses of 8 grains indicated that they had zircon compositions, and the majority of the grains were optically clear and had smooth, occasionally rounded surfaces (Figs. 2a-d). Optical microscopy on two conjoined zircon grains showed that they were milky white and completely opaque (Fig. 3a). SE imaging of these conjoined grains showed pervasive micro-fractures and possible lamellae on the crystal surfaces of both grains (Figs. 3b-d), which were not present in the other zircon grains (Figs. 2a-d). Total or partial opaqueness was also observed in some optical images of the (U-Th)/He dated apatite and zircon grains (Figs. 4a-b and d-e). Alternatively, we have evidence of clear apatite and zircon grains (Figs. 2a-d and 4c, f-j) showing little evidence of shock metamorphism.

Results: (U-Th)/He ages

Ten zircon grains gave (U-Th)/He ages ranging from 0.662 ± 0.029 to 197.3 ± 7.0 Ma (2σ), and 12 apatite (U-Th)/He analyses yielded ages ranging from 0.62 ± 0.11 to 61.5 ± 1.9 Ma (2σ, Figs. 4-5; Table 1). The three youngest ages yielded an inverse variance weighted mean age of 663 ± 28 ka (2σ; n = 3) with acceptable Mean Square of Weighted Deviates (MSWD = 2.4) and Probability (P = 9.4%) values (Fig. 5).

The 'calculated ^{4}He losses' from the 12 apatite and 10 zircon single grain analyses (Table 1) were calculated using the following equation:

$$100 - \frac{(Single\ crystal\ apatite\ or\ zircon\ Age_{corr} - 0.663\ Ma) * 100}{Oldest\ apatite\ or\ zircon\ age - 0.663\ Ma} \quad [4]$$

assuming maximum (U-Th)/He ages of 61.51 and 197.25 Ma, respectively, and 0.663 Ma as the age of the impact event (this study). The target rock lithology is volumetrically dominated by granite, and geochemical modeling of the compositions of the impactites suggested that the impact melt was derived almost exclusively from the granite target (Ukstins Peate et al. 2010), so we feel confident that the apatite and zircon grains in the impactite samples were obtained from the local granite target rock, rather than the 3.2 Ma ignimbrites. This is confirmed by the overall older (U-Th)/He ages of the apatites and zircons from the two impactites. Excluding the 4 youngest ages (0.62 ± 0.11 to 2.309 ± 0.071 Ma; 2σ), the remaining 18 (U-Th)/He analyses all yield ages older than the 3.2 Ma ignimbrite (4.69 ± 0.31 to 197.3 ± 7.0 Ma; 2σ; Table 1).

Results: Modelled impact resetting of the (U-Th)/He geochronological system

For the initial contact and compression stage (0.00027 and 0.00043 seconds at 1500 and 1600°C) the apatite minimum, maximum and average reset grain radii yielded modeled ^{4}He diffusion losses of 61-85, 34-52 and 52–76%, respectively (Table 2). For the zircon grains in the

same contact-compression stage, modeling produced much smaller ^{4}He loss values of 4.9-8.3, 3.0-5.1 and 4.0-6.7% for the respective minimum, maximum and reset grain radii (Table 2).

Modeling of ^{4}He losses in the apatites and zircons during the following adiabatic decompression shock metamorphism stage (0.1 to 1.0 seconds at 1500 and 1600°C), resulted in large ^{4}He losses of 100% in all the apatite grains (minimum, maximum and average reset radii). Similarly, the modeled zircon grains yielded high ^{4}He loss values ranging from 71-100, 49-99.7 and 62-100% for the minimum, maximum and reset grain radii, respectively (Table 2).

Discussion

The (U-Th)/He zircon and apatite mean age of 663 ± 28 ka (2σ) obtained from this study agrees within 2σ errors with the previously obtained age of 590 ± 60 ka (1σ) from quartz thermoluminescence dating, and an age range of ~500-780 ka inferred from paleomagnetic and cosmogenic nuclides studies for the Monturaqui impact crater (Verdugo and Cartes, 2000; Valenzuela et al., 2009. As both apatite and zircon (U-Th)/He analyses contribute to the youngest ages, the weighted mean age of this cluster most likely reflects the formation age of the impact structure. If the young ages had been the result of a later reheating or a slow cooling event, the distinctly different ^{4}He diffusion parameters for apatite and zircon (Farley, 2000; Reiners et al., 2004) would not have yielded overlapping young ages, thus this gives us confidence that the 663 ± 28 ka (U-Th)/He age is the Monturaqui impact structure formation age.

Milky white opaque zircon grains are a common indicator of shock metamorphism (Corfu et al., 2003). Owing to the milky opaque nature of two conjoined zircon grains in imaged but not dated grains (Fig. 3a), the presence of pervasive micro-fracturing and possible planar features or lamellae (Figs. 3b-d), plus partially or total opaque apatite grains from the (U-Th)/He

345 analyses (Figs. 4a-b, d-e), we suggest that some of the accessory minerals in the two impactite
346 samples underwent shock metamorphism. Bunch and Cassidy (1972) and Ugalde et al. (2007)
347 noted a spectrum of shock metamorphism textures in the Monturaqui impactite samples, ranging
348 from completely unshocked regions, to weak shocking (10-25 GPa) observed as micro-
349 deformation and planar features in quartz and feldspar, kinking of biotite, and multiple cleavage
350 development in apatite grains. Moderate shock levels (25-50 GPa) were identified by partly to
351 completely vitrified quartz, transformation of quartz to coesite, and conversion of feldspars to
352 maskelynite, while high shock levels (50-65 GPa) were identified by the presence of vesiculated
353 quartz and feldspar glasses, melting of biotite grains, and formation of brown and green impact
354 glasses. Therefore, our observations of both shocked and unshocked apatite and zircon grains
355 verify previous petrological observations regarding the heterogeneous nature of the shock regime
356 experienced by the Monturaqui impactite samples (Bunch and Cassidy, 1972; Ugalde et al.,
357 2007).

358 There were no observable correlations between the (U-Th)/He single crystal ages and (i)
359 optical microscope imaging of the apatite and zircon grains in terms of opaque versus clear
360 grains (Fig. 4, Table 1), (ii) the Th/U ratios (Fig. 6a), or (iii) the apatite and zircon grain radii
361 (Fig. 6b). If the compression and shock metamorphism temperatures had been uniform across the
362 impactite samples, then we would expect a more similar range of ages for the zircon and apatite
363 populations, and the smaller grains would have undergone more ^{4}He loss than the larger grains.
364 However, no correlation of the (U-Th)/He ages with grain size was observed (Fig. 6b), which
365 again indicates that the heating of the impactites was heterogeneous. The three youngest apatite
366 and zircon (U-Th)/He ages (0.616 ± 0.107 to 0.845 ± 0.183 Ma; 2σ) were sourced from the same
367 sample (CIUP 08100 with ages up to 61.5 ± 1.9 Ma; 2σ), located on the south flank of the crater

(Fig. 1). The second sample (CIUP 08099), located on the SE flank of the crater (Fig. 1) yielded older apatite and zircon ages ranging from 4.7 ± 1.7 to 197.3 ± 7.0 Ma (2σ). The 0.616-197 Ma age range in all the grains from both samples is interpreted to reflect partial to complete resetting of the (U-Th)/He ages in apatite and zircon grains, which may be due to heterogeneous heating effects (Fig. 5). These new results further substantiate the heterogeneous nature of the different pressure-temperature environments experienced by these impactite breccia samples. A regional apatite (U-Th)/He and fission track study from the nearby Salar de Atacama Basin (Henrique et al., 2018) yielded similar ages to our oldest Monturaqui apatite and zircon (U-Th)/He ages. (U-Th)/He ages from the Quimal Intrusive (~100 km NNW of Monturaqui) ranged from 38.0 ± 1.2 to 70.1 ± 3.2 Ma (2σ; n = 10), which overlap within 2σ errors with our 4 oldest (U-Th)/He apatite ages (35.6 ± 2.8 to 61.5 ± 1.9 Ma; Table 1). Apatite fission track central ages of 57 ± 13 to 170 ± 37 Ma (2σ; n = 2), collected from two samples ~ 45 km NW of Monturaqui are similar to our 3 oldest Monturaqui zircon (U-Th)/He ages of 53.5 ± 2.0 to 197.3 ± 7.0 Ma, despite the differences in the zircon He closure temperature (~200°C; Reiners et al., 2004) and the fission track annealing temperature (~120°C; zircon (U-Th)/He = ~200°C; Ketcham et al., 1999). Therefore, the Henrique et al. (2018) apatite (U-Th)/He and fission-track regional cooling ages verify our oldest apatite and zircon (U-Th)/He ages, and gives us confidence in our calculated % ^{4}He loss values (Table 1), which are directly compared to our modeled % ^{4}He loss values (Table 2; Fig. 7).

Comparing modeled amounts of ^{4}He loss at temperatures of 1500 and 1600°C from the (i) initial contact and compression and (ii) the adiabatic decompression and shock metamorphism stages indicates that the latter is probably the main contributor to the partial to complete resetting of the (U-Th)/He apatite and zircon ages in the Monturaqui impactites (Fig. 7). This is especially

391 true for the zircons, as ^{4}He diffusion is observably slower in zircon compared to apatite (Fig. 8),
392 and only the longer duration shock metamorphism stage is capable of producing 100% ^{4}He
393 resetting in zircons (Fig. 7).

394 Modeling of ^{4}He losses in 25 and 50 µm apatite and zircon grains (commonly utilized for
395 (U-Th)/He dating), at temperatures of 1500 and 1600°C, indicates that the very short duration
396 (0.3-0.4 milliseconds) initial contact and compression stage is insufficient to completely reset
397 (U-Th)/He systematics (Figs. 7-8; Table 2). A contact and compression stage duration of >0.51
398 seconds with a temperature of 1600°C would be sufficient to reset the (U-Th)/He systematics in
399 25 and 50 µm radii apatites and smaller zircon grains (25 µm radius; Fig. 8). However, this
400 would require a very large impactor (~9.3 km diameter) resulting in final rim-to-rim impact
401 crater diameters of ~130-290 km (using projectile and target rock densities of 1.5-8.0 g/cm^3 in
402 the *Crater* software (Melosh and Beyer, 2002)).

403 In contrast, modelling of the longer duration (1.4-0.76 seconds at 1500 and 1600°C,
404 respectively) decompression and shock metamorphism stage at Monturaqui indicates that it is
405 capable of causing ^{4}He losses of 100% in apatites and 49-100% in zircons (Fig 7; Table 2). This
406 agrees relatively well with the calculated ^{4}He losses of 14-100 and 28-100% in the Monturaqui
407 apatites and zircons, respectively (Fig. 7). The large variability of the shock levels in
408 Monturaqui impactite samples could also explain the observed range of partial to total resetting
409 in the (U-Th)/He apatite and zircon ages (Figs. 5 and 7).

410 Assuming temperatures of 1500 and 1600°C during both the compression and shock
411 metamorphism stages, ^{4}He loss modeling of the reset zircon grain (grain # z003; 30.5 µm radius;
412 Table 1) yields combined compression and shock metamorphism durations of 1.4 to 0.76
413 seconds to achieve 100% ^{4}He loss, respectively (Fig. 8). If the 55.4-99.6% calculated ^{4}He losses

414 in the remaining 8 zircon grains (ignoring the 0% loss zircon grain, which requires a temperature
415 of <270°C) are assumed to be due to temperature inhomogeneities in the two samples, then
416 reverse modeling of the calculated % ^{4}He losses and grain radii from each of the (U-Th)/He
417 analyses (Table 1) yields a temperature range of 1015-1529°C, which would be equivalent to
418 shock pressures of 50-60 GPa (Stöffler et al., 2018) in the two impactite samples. Similar reverse
419 modelling of the 14.0-100% calculated ^{4}He losses in the 11 analysed apatite grains (ignoring the
420 0% loss apatite grain, which requires a temperature of <210°C) yields a lower temperature range
421 of 512-902°C, which is equivalent to lower shock pressures of 35-45 GPa (Stöffler et al., 2018).
422 We have shown that the (U-Th)/He method can be successfully applied to the dating of
423 variably shocked impactite samples from impact structures, including very small <1 km diameter
424 craters, which have thus far yielded few geochronological ages due to lack of suitable material
425 for the more routinely used U-Pb and ^{40}Ar-^{39}Ar techniques (i.e., impact melts or tektites). Based
426 on this study and previous (U-Th)/He studies of impact structures (van Soest et al., 2011; Wartho
427 et al., 2012; Young et al., 2013; Wielicki et al. 2014; Biren et al., 2014, 2016, 2019), we
428 recommend analyzing numerous single grains (i.e., >20-30), especially for non-impact melt
429 material, distal ejecta, and smaller impact structures, where only ~10 % of grains are found to be
430 reset. We also recommend analyzing multiple mineral phases to confirm the validity of the
431 youngest ages as impact event ages.
432
433 **Conclusions**
434 The 350 m diameter Monturaqui impact structure has been dated at 663 ± 28 ka (2σ)
435 using the (U-Th)/He geochronological technique. The dating method is capable of expanding the
436 field of geochronologically datable impact materials and successfully determining accurate ages

437 from very small (<1 km diameter) impact structures, by utilizing the relatively rapid diffusion
438 and low-temperature resetting properties of the ^{4}He daughter product in U- and Th-bearing
439 minerals.

440 Modeling of ^{4}He losses in apatite and zircon grains from the Monturaqui impact crater
441 suggests that the short duration initial contact and compression stage is not capable of causing
442 sufficient resetting of the (U-Th)/He ages, especially in the more retentive zircons. However, the
443 longer duration adiabatic decompression and shock metamorphism stage can cause complete
444 resetting of the (U-Th)/He systematics in both apatite and zircon grains from this 350 m diameter
445 impact structure.

Acknowledgements

IAU would like to acknowledge support from NSF grant EAR-1126728, NASA grant 06-PGG06-6, University of Iowa CLAS start-up funds and the University of Iowa Obermann Center for support during fieldwork and manuscript preparation. J-AW, MvS, MBB and KVH would like to acknowledge the support of NSF grant EAR-0948143. We would also like to thank Dr Henrietta E. Cathey (LeRoy Eyring Center for Solid State Science, ASU) for assistance in obtaining the secondary electron images presented in this paper. We also gratefully acknowledge the field assistance of Christy Kloberzanz, Sarah Byram and David W. Peate. We thank Barry Kohn and an anonymous reviewer for their careful reviews and the editorial handling of Robyn Pickering, which improved the quality of this research paper.

References

Beck, P., Ferroir, T., Gillet, P., 2007. Shock-induced compaction, melting, and entrapment of atmospheric gases in Martian meteorites. Geophy. Res. Lett. 34, L01203. https://doi.org/10.1029/2006GL028141

Bhatnagar, V.M., 1969. The melting points of synthetic apatites. Mineral. Mag. 37, 527-528. https://doi.org/10.1180/minmag.1969.037.288.20

Biren, M.B., van Soest, M., Wartho, J-A., Spray, J.G., 2014. Dating the cooling of exhumed central uplifts of impact structures by the (U-Th)/He method: A case study at Manicouagan. Chem. Geol. 377, 56-71. https://doi.org/10.1016/j.chemgeo.2014.03.013

Biren, M.B., van Soest, M.C., Wartho, J-A., Hodges, K.V., Spray, J.G., 2016. Diachroneity of the Clearwater West and Clearwater East impact structures indicated by the (U-Th)/He dating method. Earth Planet. Sci. Lett. 453, 56-66. https://doi.org/10.1016/j.epsl.2016.07.053

Biren, M.B., Wartho, J-A., van Soest, M.C., Hodges, K.V., Cathey, H., Glass, B.P., Koeberl, C., Horton Jr., J.W., Hale, W., 2019. (U-Th)/He zircon dating of Chesapeake Bay distal impact ejecta from ODP site 1073. Meteorit. Planet. Sci. 54, 1840-1852. https://doi.org/10.1111/maps.13316

Bogard, D., Hörz, F., Stöffler, D., 1988. Loss of radiogenic argon from shocked granitic clasts in suevite deposits from the Ries Crater. Geochim. Cosmochim. Acta 52, 2639-2649. https://doi.org/10.1016/0016-7037(88)90032-4

Buchwald, V.F., 1975. Handbook of iron meteorites: Their history, distribution, composition and structure (3 volumes). University of California Press, Berkeley, CA, USA.

Bunch, P., Cassidy, W., 1972. Petrographic and electron microprobe study of the Monturaqui impact. Cont. Mineral. Petrol. 36, 95-112. https://doi.org/10.1007/BF00371181

Collins, G.S., Melosh, H.J., Marcus, R.A., 2005. Earth impact effects program: A web-based computer program for calculating the regional environmental consequences of a meteoroid impact on Earth. Meteorit. Planet. Sci. 40, 817-840. https://doi.org/10.1111/j.1945-5100.2005.tb00157.x

Crank, J., 1975. The Mathematics of Diffusion: Oxford University Press, London, pp. 414.

Corfu, F., Hanchar, J.M., Hoskin, P.W.O., Kinny, P., 2003. Atlas of zircon textures. In *Zircon*, Hanchar, J.M., Hoskin P.W.O. (editors), Mineralogical Society of America, Washington, D.C. Rev. Mineral. Geochem. 53, 469–500. https://doi.org/10.2113/0530469

Deutsch, A., Schärer, U., 1994. Dating terrestrial impact events. Meteoritics 29, 301-322. https://doi.org/10.1111/j.1945-5100.1994.tb00595.x

Earth Impact Database, 2021. Planetary and Space Science Centre, University of New Brunswick, http://www.passc.net/EarthImpactDatabase/New%20website_05-2018/Index.html, accessed June 2020.

Evans, N.J., Byrne, J.P., Keegan, J.T., Dotter, L.E., 2005. Determination of uranium and thorium in zircon, apatite, and fluorite: Application to laser (U-Th)/He thermochronology. J. Analytic. Chem. 60, 1159-1165. https://doi.org/10.1007/s10809-005-0260-1

Farley, K.A., 2000, Helium diffusion from apatite: General behavior as illustrated by Durango fluorapatite. J. Geophys. Res. 106, B2, 2903-2914. https://doi.org/10.1029/1999JB900348

497 Farley, K.A., Wolf, R.A., Silver, L.T., 1996. The effects of long alpha-stopping distances on (U-
498 Th)/He ages. Geochim. Cosmochim. Acta 60, 4223-4229. https://doi.org/10.1016/S0016-
499 7037(96)00193-7

500 Finch, R.J., Hanchar, J.M., 2003. Structure and chemistry of zircon and zircon-group minerals.
501 In *Zircon*, Hanchar, J.M., Hoskin P.W.O. (eds.), Mineralogical Society of America,
502 Washington, D.C. Rev. Mineral. Geochem. 53, 1-25. https://doi.org/10.2113/0530001

503 French, B.M., 1998. Traces of catastrophes: A handbook of shock-metamorphic effects in
504 terrestrial meteorite impact structures. Lunar Planet. Inst. Contrib. 954, pp. 120.

505 Gillet, P., El Goresy, A., 2013. Shock events in the Solar System: The message from minerals in
506 terrestrial planets and asteroids. Ann. Rev. Earth Planet. Sci. 41, 257-285.
507 https://doi.org/10.1146/annurev-earth-042711-105538

508 Grieve, R.A.F., Cintala, M.J. 1977. Planetary differences in impact melting. Adv. Space Res. 20,
509 1551-1560. https://doi.org/10.1016/S0273-1177(97)00877-6

510 Gurov, E.P., Gurova, E.P., 1998. The group of Macha craters in western Yakutia. Planet. Space
511 Sci. 46, 323-328. https://doi.org/10.1016/S0032-0633(97)00041-X

512 Henrique, S., DeCelles, P.G., Carrapa, B., 2018. Cretaceous to Middle Cenozoic exhumation
513 history of the Cordillera de Domeyko and Salar de Atacama Basin, northern Chile. Tectonics
514 38, 395-416. https://doi.org/10.1029/2018TC005203

515 Holsapple, K.A., 2020. Computer program *Impact and Explosion Effects*, v. 4.02, University of
516 Washington, Seattle, USA (available at
517 http://keith.aa.washington.edu/craterdata/scaling/index.htm).

518 Hourigan, J.K., Reiners, P.W., Brandon, M.T., 2005. U-Th zonation-dependent alpha-ejection in
519 (U-Th)/He chronometry. Geochim. Cosmochim. Acta 69, 3349-3365.
520 https://doi.org/10.1016/j.gca.2005.01.024

521 Kelley, S.P., Gurov, E., 2002. Boltysh, another end-Cretaceous impact. Meteroit. Planet Sci. 37,
522 1031-1043. https://doi.org/10.1111/j.1945-5100.2002.tb00875.x

523 Ketcham, R.A., Donelick, R.A., Carlson, W.D., 1999. Variability of apatite fission-track
524 annealing kinetics: III. Extrapolation to geological time scales. Am. Mineral. 84, 1235-1255.
525 https://doi.org/10.2138/am-1999-0903

526 Kloberdanz, C.M., 2010. Geochemical analysis of the Monturaqui impact crater, Chile. MSc
527 thesis, University of Iowa, USA. https://doi.org/10.17077/etd.x9hrqulb

528 Kring, D.A., Tikoo, S.M., Schmieder, M., Riller, U., Rebolledo-Vieyra, M., Simpson, S.L.,
529 Osinski, G.R., Gattacceca, J., Wittmann, A., Verhagen, C.M., Cockell, C.S., Coolen, M.J.L.,
530 Longstaffe, F.J., Gulick, S.P.S., Morgan, J.V., Bralower, T.J., Chenot, E., Christeson, G.L.,
531 Claeys, P., Ferrière, L., Gebhardt, C., Goto, K., Green, S.L., Jones, H., Lofi, J., Lowery,
532 C.M., Ocampo-Torres, R., Perez-Cruz, L., Pickersgill, A.E., Poelchau, M.H., Rae, A.S.P.,
533 Rasmussen, C., Sato, H., Smit, J., Tomioka, N., Urrutia-Fucugauchi, J., Whalen, M.T., Long,
534 X., Yamaguchi, K.E., 2020. Probing the hydrothermal system of the Chicxulub impact crater.
535 Science Advances 6. https://doi.org/10.1126/sciadv.aaz3053

536 Hodych, J.P., Dunning, G.R., 1992. Did the Manicouagan impact trigger end-of-Triassic mass
537 extinction? Geology 20, 51-54. https://doi.org/10.1130/0091-
538 7613(1992)020<0051:DTMITE>2.3.CO;2

539 Melosh, H.J., Beyer, R.A., 2020. Computer program *Crater*, University of Purdue, West
540 Lafayette, Indiana, USA (available at
541 https://www.eaps.purdue.edu/impactcrater/crater_c.html).

542 Mpodozis, C.M., Herve, F.A., Davidson, J.M., Rivano, S.G., 1983. Los granitoides de Cerros de
543 Lila, manifestaciones de un epidodio intrusive y termal del Paleozioco inferior en los Andes
544 del norte de Chile. Rev. Geol. Chile 18, 3-14. http://dx.doi.org/10.5027/andgeoV10n1-a01

545 Nakamura, A., Yokoyama, Y., Sekine, Y., Goto, K., Komatsu, G., Senthil Kumar, P., Matsuzaki,
546 H., Kaneoka, I., Matsui, T., 2014. Formation and geomorphologic history of the Lonar
547 impact crater deduced from in situ cosmogenic ^{10}Be and ^{26}Al. Geochem., Geophys., Geosyst.
548 15, 3190-3197. https://doi.org/10.1002/2014GC005376

549 Newsom, H.E., Graup, G., Sewards, T., Keil, K., 1986. Fluidization and hydrothermal alteration
550 of the suevite deposit at the Ries crater, West Germany, and implications for Mars. J.
551 Geophy. Res. Solid Earth 91, E239-E251. https://doi.org/10.1029/JB091iB13p0E239

552 Parnell, J., Osinski, G.R., Lee, P., Green, P.F., Baron, M.J., 2005. Thermal alteration of organic
553 matter in an impact crater and the duration of postimpact heating. Geology 33, 373-376.
554 https://doi.org/10.1130/G21204.1

555 Ramirez, C.F., Gardeweg, M., 1982. Carta Geológica de Chile 1:250,000, Hoja Toconao.
556 Servicio Nacional de Geologica y Mineria, Santiago de Chile, 54.

557 Rassmussen, C., Stockli, D.F., Ross, C.H., Pickersgill, A., Gulick, S.P., Schmieder, M.,
558 Christeson, G.L., Wittmann, A., Kring, D.A., Morgan, J.V., and the IODP-ICDP Expedition
559 364 Science Party, 2019. U-Pb memory behavior in Chicxulub's peak ring – Applying U-Pb
560 depth profiling to shocked zircon. Chem. Geol. 525, 356-367.
561 https://doi.org/10.1016/j.chemgeo.2019.07.029

562 Rathbun, K., Ukstins, I., Drop. S., 2017. Monturaqui meteorite impact crater, Chile: A field test
563 of the utility of satellite-based mapping of ejecta at small craters. Amer. Geophy. Union Fall
564 meeting, 11-15 December 2017, New Orleans, Louisiana, USA, abstract #EP53B-1731.

565 Reiners, P.W., Spell, T.L., Nicolescu, S., Zanetti, K.A., 2004. Zircon (U-Th)/He
566 thermochronometry: He diffusion and comparisons with $^{40}Ar/^{39}Ar$ dating. Geochim.
567 Cosmochim. Acta 68, 1857-1887. https://doi.org/10.1016/j.gca.2003.10.021

568 Reiners, P.W., 2005. Zircon (U-Th)/He Thermochronometry. In *Zircon*, Hanchar, J.M., Hoskin
569 P.W.O. (eds.), Mineralogical Society of America, Washington, D.C. Rev. Mineral. Geochem.
570 58, 151-179. https://doi.org/10.2138/rmg.2005.58.6

571 Salminen, J., Donadini, F., Pesonen, L.J., Masaitis, V.L., Naumov, M.V., 2006. Paleomagnetism
572 and petrophysics of the Jänisjärvi impact structure, Russian Karelia. Meteorit. Planet. Sci. 41,
573 1853-1870. https://doi.org/10.1111/j.1945-5100.2006.tb00456.x

574 Sanchez, J., Cassidy, W., 1966. A previously undescribed meteorite crater in Chile. J. Geophys.
575 Res. 71, 4891-4895. https://doi.org/10.1029/JZ071i020p04891

576 Schärer, U., Deutsch, A., 1990. Isotope systematics and shock-wave metamorphism: II. U-Pb
577 and Rb-Sr in naturally shocked rocks; the Haughton Impact Structure, Canada. Geochim.
578 Cosmochim. Acta, 54 3435-3447. https://doi.org/10.1016/0016-7037(90)90296-W

579 Schmieder, M., Kring, D.A., 2020. Earth's impact events through geological time: A list of
580 recommended ages for terrestrial impact structures and deposits. Astrobio. 20.
581 https://doi.org/10.1089/ast.2019.2085

582 Schwenzer, S.P., Fritz, J., Stöffler, D., Trieloff, M., Amini, M., Greshanke, A., Herrmann, S.,
583 Herwig, K., Jochum, K.P., Mohapatra, R.K., Stoll, B., Ott, U., 2008. Helium loss from

584 Martian meteorites mainly induced by shock metamorphism: Evidence from new data and a
585 literature compilation. Meteorit. Planet. Sci. 43, 1841-1859. https://doi.org/10.1111/j.1945-
586 5100.2008.tb00647.x
587 Shaw, C.S.J., Walton, E., 2013. Thermal modeling of shock melts in Martian meteorites:
588 Implications for preserving Martian atmospheric signatures and crystallization of high-
589 pressure minerals from shock melts. Meteorit. Planet. Sci. 48, 758-770.
590 https://doi.org/10.1111/maps.12100
591 Sighinolfi, G.P., Sibilia, E., Contini, G., Martini, M., 2015, Thermoluminescence dating of the
592 Kamil impact crater (Egypt), Meteorit. Planet. Sci. 50. https://doi.org/10.1111/maps.12417
593 Stöffler, D., Hamann, C., Metzler, K., 2018. Shock metamorphism of planetary silicate rocks and
594 sediments: Proposal for an updated classification system. Meteorit. Planet. Sci., 53, 5-49.
595 https://doi.org/10.1111/maps.12912
596 Ugalde, H., Valenzuela, M., Milkereit, B., 2007. An integrated geophysical and geological study
597 of the Monturaqui impact crater, Chile. Meteorit. Planet. Sci. 42, 2153-2163.
598 https://doi.org/10.1111/j.1945-5100.2007.tb01015.x
599 Ukstins Peate, I., Kloberdanz, C., Peate, D.W., Chung Wan, L., Cabrol, N., Grin, E., Piatek, J.,
600 Chong, G., 2010. Non-modal melting of target rocks to produce impactite at Monturaqui
601 Crater, Chile. 41st Lunar Planet. Sci. Conf., 1-5 March 2010, Houston, Texas, USA, Lunar
602 Planet. Inst. Contrib. No. 1533, p. 2089.
603 Valenzuela, M., Bourlès, D.L., Braucher, R., Faestermann, T., Finkel, R.C., Gattacceca, J.,
604 Korschinek, G., Merchel, S., Morata, D., Poutivtsev, M., Rochette, P., Rugel, G., Sauvet, C.,
605 2009. New age estimation of the Monturaqui impact crater: 72nd Met. Soc. Conf., 13-18 July
606 2009, Nancy, France, abstract #5185.

van Soest, M. C., Hodges, K. V., Wartho, J.-A., Biren, M. B., Monteleone, B. D., Ramezani, J., Spray, J.G., Thompson, L.M., 2001. (U/Th)/He dating of terrestrial impact structures: The Manicouagan example. Geochem. Geophys. Geosyst. 12, QOAA16. https://doi.org/10.1029/2010GC003465

Verdugo, M., Cartes, C., 2000, Establecimiento de la edad del crater Monturaqui por el metodo termoluminicencia en solidos: Faculty de Fisica Report, Pontifica Universidad Catolica de Chile, 1-18.

Veski, S., Heinsalu, A., Lang, V., Kestlane, Ü., Possnert, G., 2004, The age of the Kaali meteorite craters and the effect of the impact on the environment and man: Evidence from inside the Kaali craters, island of Saaremaa, Estonia, Veget. Hist. Archaeobot. 13, 197-206. https://doi.org/10.1007/s00334-004-0043-x

Walton, E., Shaw. C.S.J., Cogswell, S., Spray, J. G. 2006. Crystallization rates of shock melts in three Martian basalts: Experimental simulation with implications for meteoroid dimensions. Geochim. Cosmochim. Acta 70, 1059–1075. https://doi.org/10.1016/j.gca.2005.10.033

Wartho, J-A., Kelley, S.P., 2003. $^{40}Ar/^{39}Ar$ ages in mantle xenolith phlogopites: Determining the ages of multiple lithospheric mantle events and diatreme ascent rates in southern Africa and Malaita, Solomon Islands. In *Geochronology: Linking the Isotopic Record with Petrology and Textures*, Vance, D., Müller, W., Villa, I.M. (eds.), Geol. Soc. Lond. Spec. Pubs. 220, 231-248. https://doi.org/10.1144/GSL.SP.2003.220.01.14

Wartho, J-A., van Soest, M.C., King, D.T. Jr., Petruny, L.W., 2012. An (U-Th)/He geochronological age for the shallow-marine Wetumpka impact structure, Alabama, USA, Meteorit. Planet. Sci. 47, 1243-1255. https://doi.org/10.1111/j.1945-5100.2012.01381.x

Wielicki, M.M., Harrison, T.M., Schmitt, R.T., Stöffler, D., 2014. Dating terrestrial impact structures: U-Pb depth profiles and (U-Th)/He ages of zircon. Geophy. Res. Lett. 41, 433-454. https://doi.org/10.1002/2014GL060757

Wünnemann, K., Zhu, M-H., Stöffler, D., 2016. Impacts into quartz sand: Crater formation, shock metamorphism, and distribution in laboratory experiments and numerical models. Meteorit. Planet. Sci. 51, 1762-1794. https://doi.org/10.1111/maps.12710

Young, K.E., van Soest, M.C., Hodges, K.V., Watson, E.B., Adams, B.A., Lee. P., 2013. Impact thermochronology and the age of Haughton impact structure, Canada. Geophy. Res. Lett. 40, 3836-3840. https://doi.org/10.1002/grl.50745

638 **Figure and table captions**

639 **Fig. 1.** (a) The location of Monturaqui impact structure in Northern Chile is shown with a star.
640 (b) Geologic map of Monturaqui with two marked impactite sample locations (circles) that were
641 selected for (U-Th)/He dating. The asymmetric base of crater is filled with lake sediment
642 deposits. After Ugalde et al. (2007), Ukstins Peate et al. (2010) and Rathbun et al. (2017).
643 **Fig. 2.** Optical (small white boxed images) and secondary electron photomicrographs of four
644 unshocked zircon grains from impactite samples CIUP 08099 (a-b) and CIUP 08100 (c-d).
645 **Fig. 3.** (a) Optical and (b-d) secondary electron photomicrographs of shocked conjoined zircon
646 crystals (CIUP 08099). The white boxes in Fig. 3b indicate the positions of the
647 photomicrographs shown in Figs. 3c-d. The dashed black and white lines in Figs. 3c-d indicate a
648 conjugate network of subplanar and occasionally curved micro-fractures (2-13 μm in length),
649 and the black arrows indicate lamellae-like features (2 μm in length) in these zircon grains.
650 **Fig. 4.** Optical photomicrographs (a-j) of some (U-Th)/He dated apatite and zircon grains from
651 the two impactite samples, with associated (U-Th)/He ages and 2σ uncertainties, and grain
652 lengths and diameters.
653 **Fig. 5.** Relative probability plots for (U-Th)/He single crystal apatite and zircon ages from two
654 impactite samples. The dashed box in the main plot indicates the area demarked for the more
655 detailed insert plot of the younger 0-10 Ma (U-Th)/He ages.
656 **Fig. 6.** (a) Th/U ratios versus (U-Th)/He single crystal ages for apatites and zircons. (b) Apatite
657 and zircon grain radii (R2 in Table 1) versus (U-Th)/He single crystal ages. The squares indicate
658 the 3 youngest apatite and zircon (U-Th)/He ages used to calculate the Monturaqui weighted
659 mean impact age.
660

Fig. 7. Comparison of (a) modeled % ^{4}He losses (Table 2) from zircon and apatite grains during the initial contact and compression stage (0.27-0.43 milliseconds duration at 1500 and 1600°C), and the adiabatic decompression and shock metamorphism stage (0.1-1 seconds duration at 1500 and 1600°C), versus (b) calculated % ^{4}He losses (Table 1) for the Monturaqui impact structure.

Fig. 8. Modeled % ^{4}He loss from the 25 and 50 µm radii apatite (black areas) and zircon (grey areas) grains typically used for (U-Th)/He analysis, heated from 1500-1600°C for varying durations. 100% ^{4}He losses would be achieved with impact heating durations of 0.93 to 0.51 seconds (25µm radius zircon) and 3.7 to 2.0 seconds (50µm radius zircon), at 1500 and 1600°C, respectively. Much shorter durations are required to achieve 100% ^{4}He losses in apatites - 0.0028 to 0.0017 (25 µm radius) and 0.011 to 0.0068 seconds (50 µm radius) at 1600 and 1500°C, respectively. * = Modeling of the 30.5 µm radius 100% reset zircon grain (Table 1) from Monturaqui, yielding 100% ^{4}He losses with durations of 1.4 seconds (1500°C) and 0.76 seconds (1600°C).

Table 1. (U-Th)/He geochronological analyses of apatites and zircons from the Monturaqui impact crater.

Table 2. Modeling of ^{4}He loss from apatite and zircon grains during Monturaqui impact crater-forming stages.

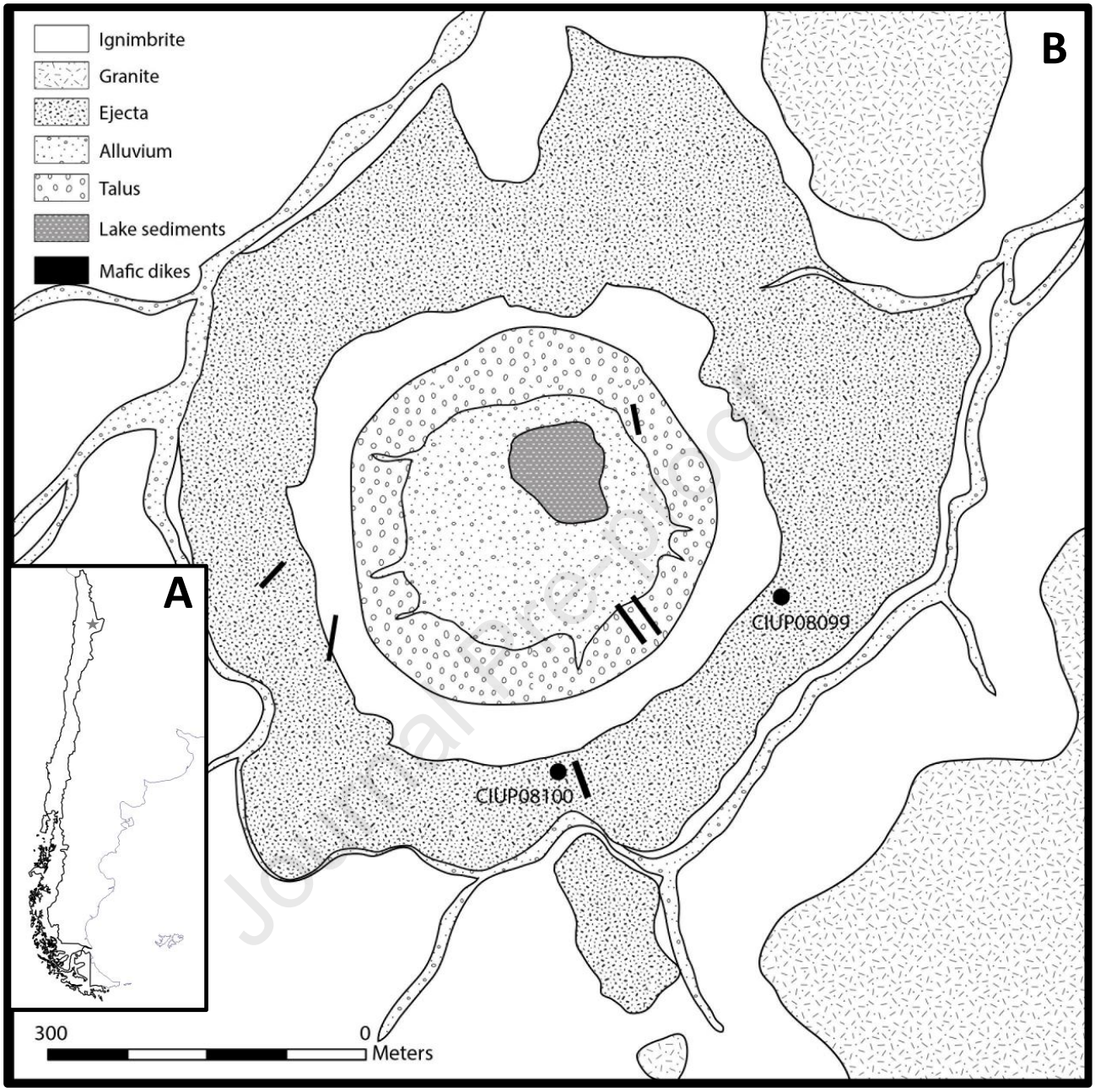
Ignimbrite
Granite
Ejecta
Alluvium
Talus
Lake sediments
Mafic dikes
B
A
CIUP08099
CIUP08100
300
0
Meters

Fig. 1

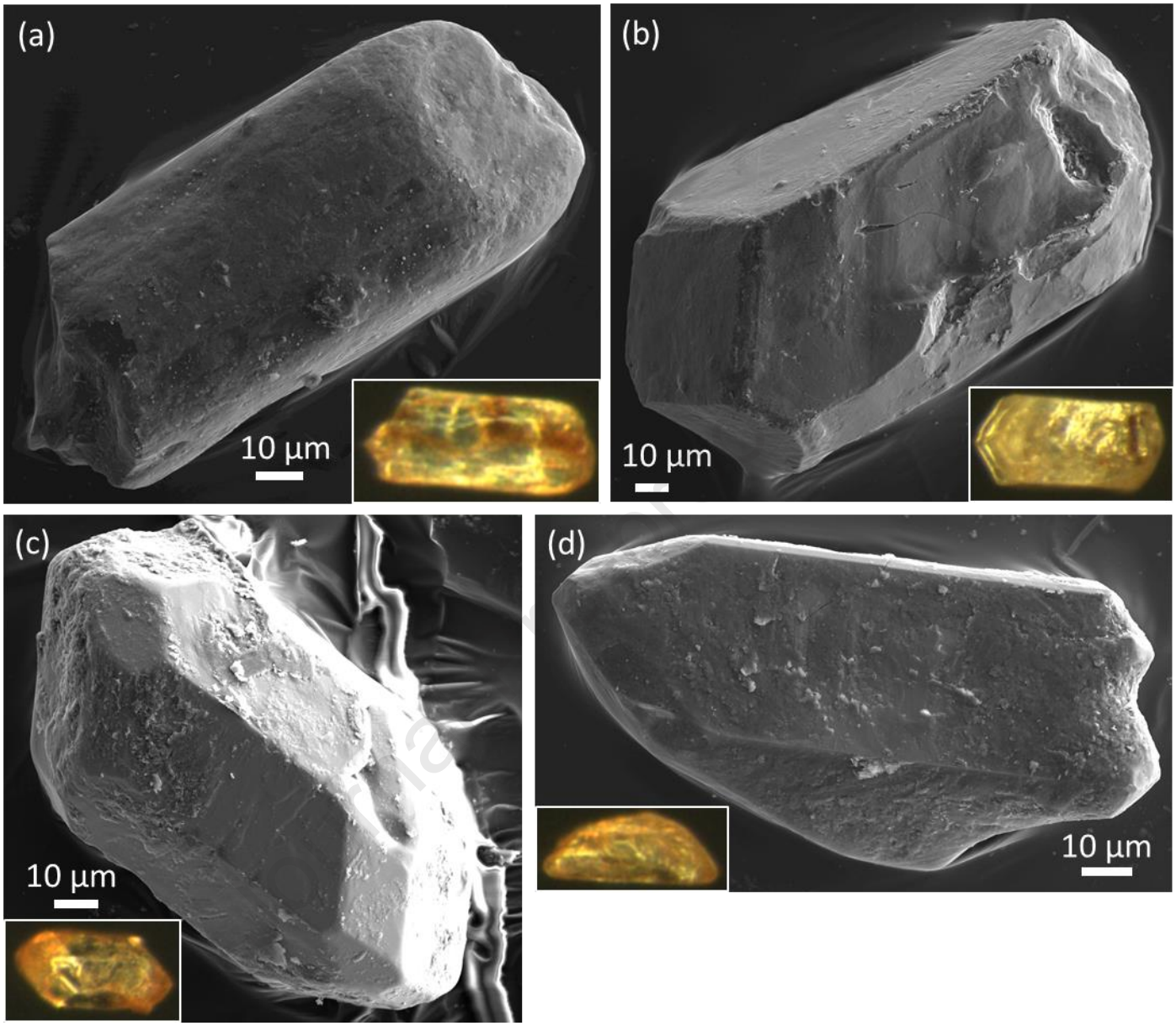

Fig. 2

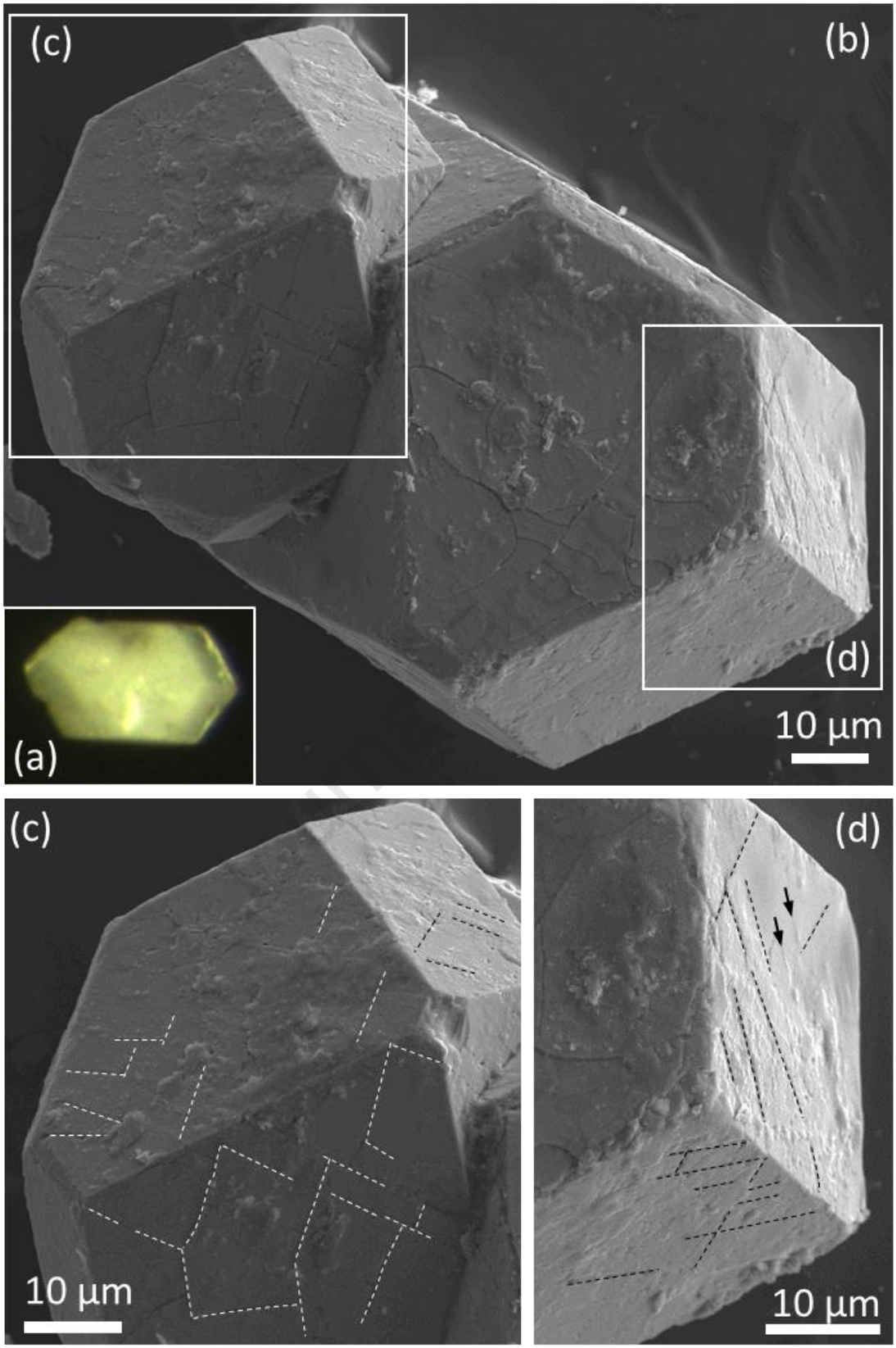

Fig. 3

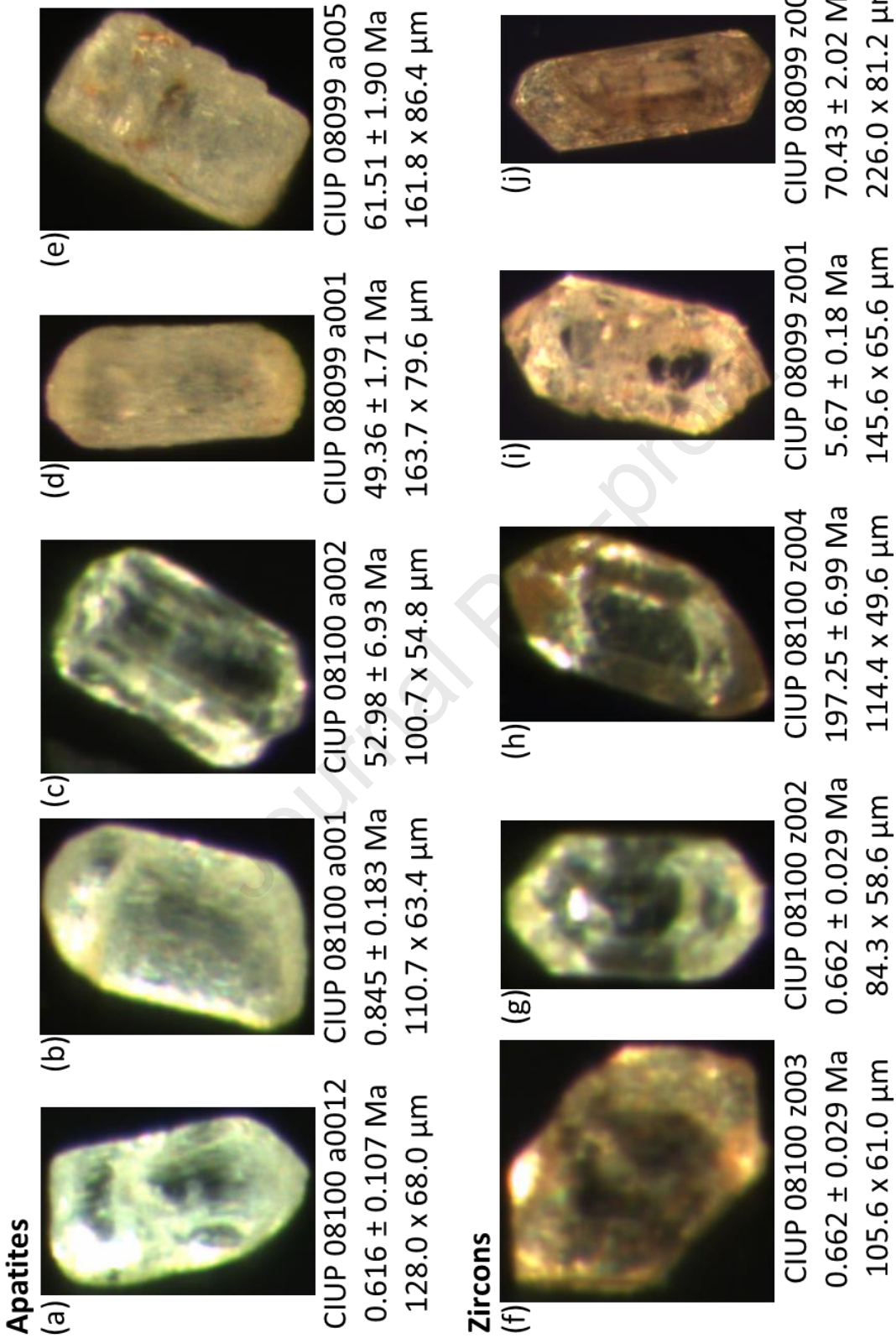
Apatites
(a)
(b)
(c)
(d)
(e)
CIUP 08100 a0012
0.616 ± 0.107 Ma
128.0 x 68.0 µm
CIUP 08100 a001
0.845 ± 0.183 Ma
110.7 x 63.4 µm
CIUP 08100 a002
52.98 ± 6.93 Ma
100.7 x 54.8 µm
CIUP 08099 a001
49.36 ± 1.71 Ma
163.7 x 79.6 µm
CIUP 08099 a005
61.51 ± 1.90 Ma
161.8 x 86.4 µm
Zircons
(f)
(g)
(h)
(i)
(j)
CIUP 08100 z003
0.662 ± 0.029 Ma
105.6 x 61.0 µm
CIUP 08100 z002
0.662 ± 0.029 Ma
84.3 x 58.6 µm
CIUP 08100 z004
197.25 ± 6.99 Ma
114.4 x 49.6 µm
CIUP 08099 z001
5.67 ± 0.18 Ma
145.6 x 65.6 µm
CIUP 08099 z002
70.43 ± 2.02 Ma
226.0 x 81.2 µm

Fig. 4

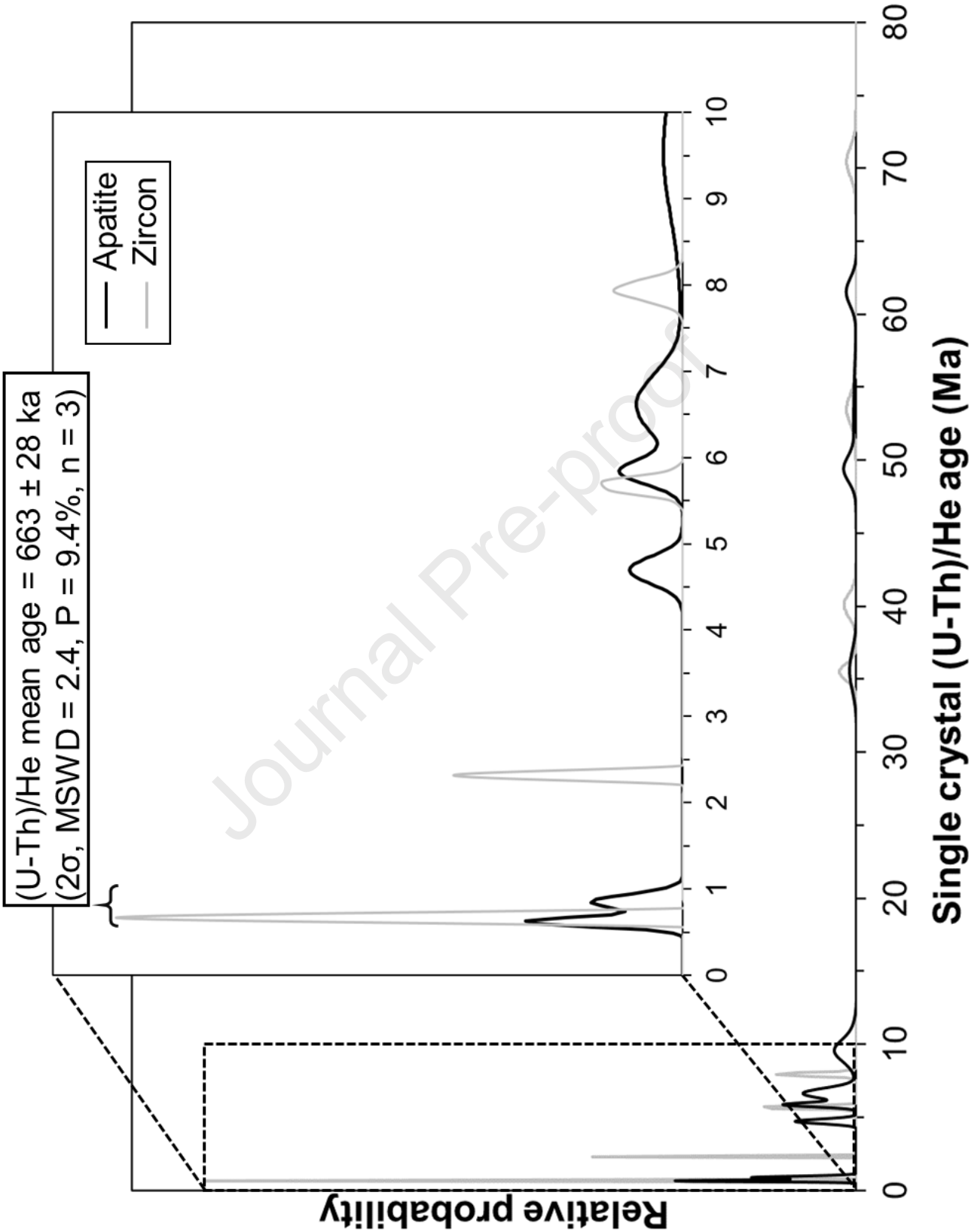
(U-Th)/He mean age = 663 ± 28 ka
(2σ, MSWD = 2.4, P = 9.4%, n = 3)
Apatite
Zircon
Relative probability
Single crystal (U-Th)/He age (Ma)
0
10
20
30
40
50
60
70
80
0
1
2
3
4
5
6
7
8
9
10

Fig. 5

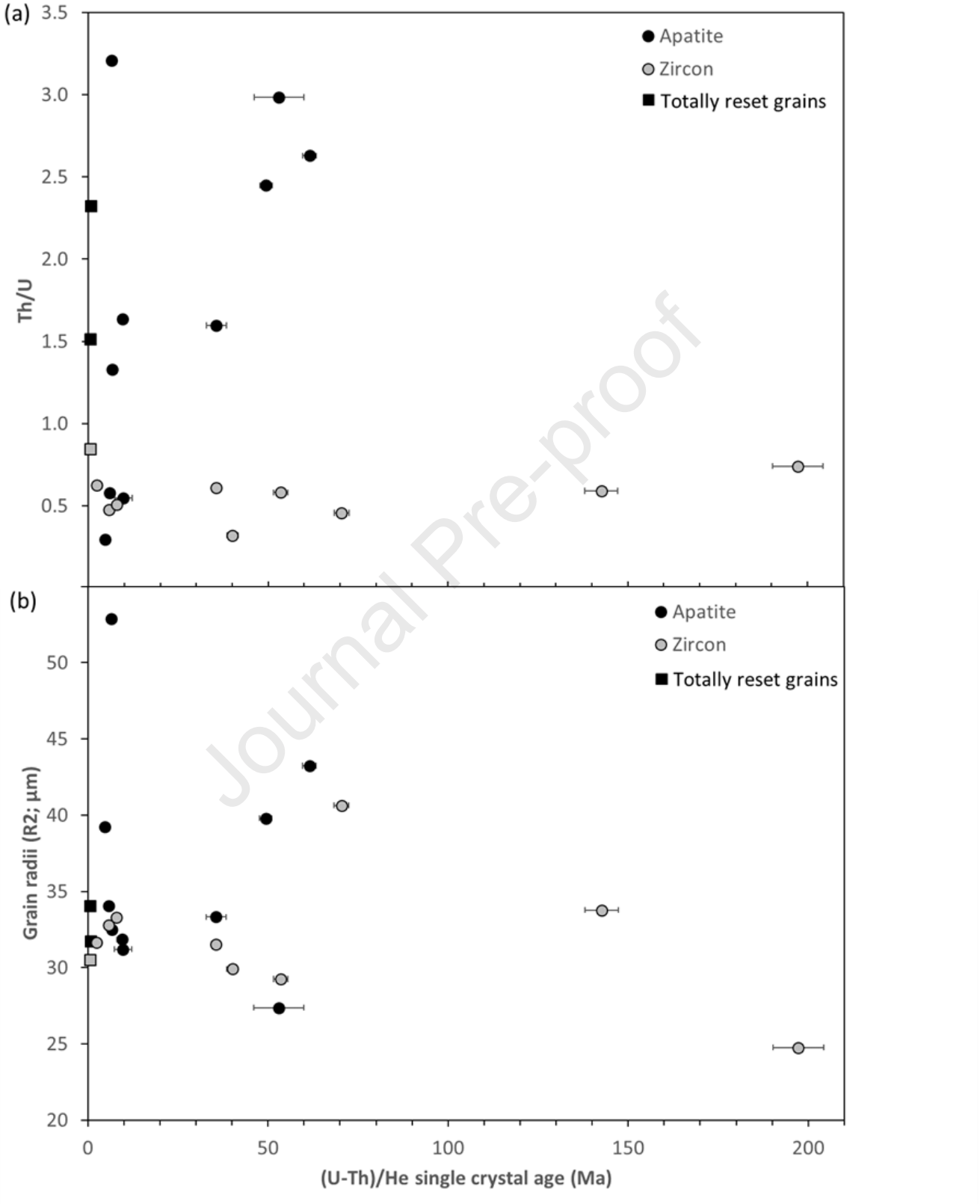
(a)
Apatite
Zircon
Totally reset grains
Th/U
3.5
3.0
2.5
2.0
1.5
1.0
0.5
(b)
Apatite
Zircon
Totally reset grains
Grain radii (R2; µm)
50
45
40
35
30
25
20
0
50
100
150
200
(U-Th)/He single crystal age (Ma)

Fig. 6

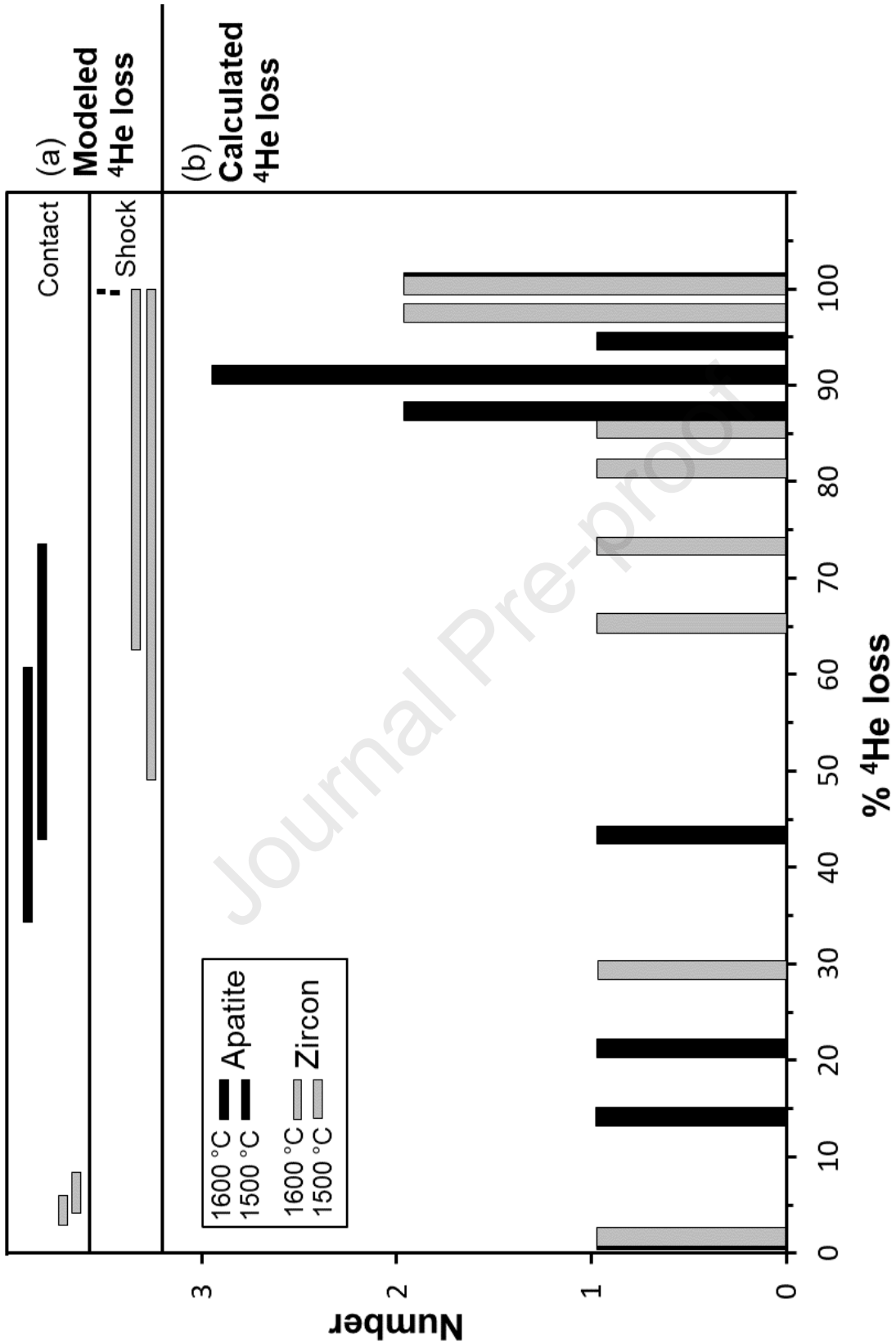

Fig. 7

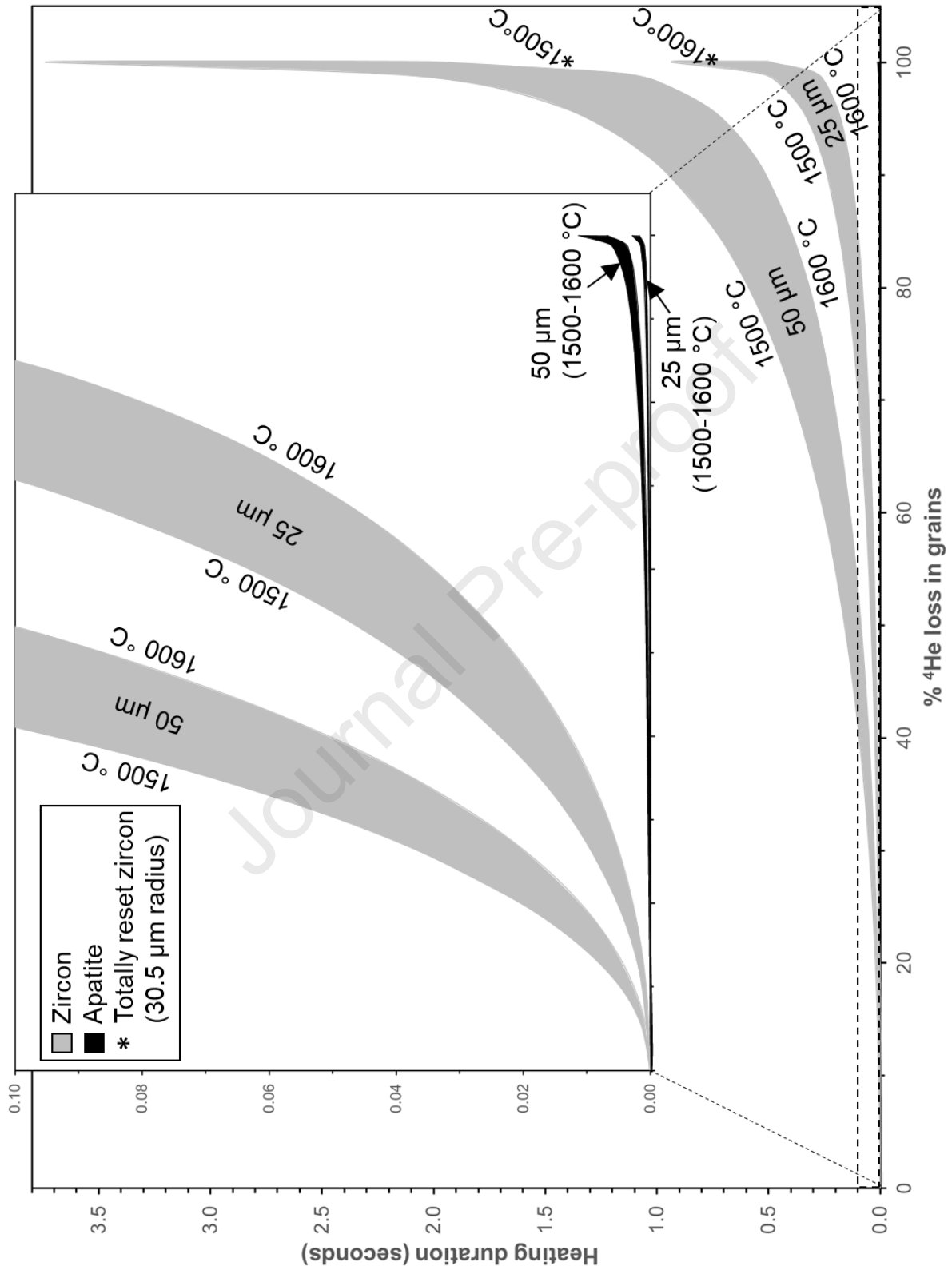
Heating duration (seconds)
% 4He loss in grains
Zircon
Apatite
* Totally reset zircon (30.5 µm radius)
1500 °C
50 µm
1600 °C
25 µm
1500 °C
1600 °C
50 µm (1500-1600 °C)
25 µm (1500-1600 °C)
1500 °C
50 µm
1600 °C
25 µm
1500 °C
1600 °C
*1600°C
*1500°C

Fig. 8

Table 1: (U-Th)/He geochronolgical analyses of apatites and zircons from the Monturaqui impact crater

Sample	Grain#[a]	[^{238}U][b]	Error[c]	[^{232}Th][b]	Error[c]	Th/U	[^{4}He][b,d]	Error[c]	Age$_{raw}$[e]	Error[c]	R1[f]	R2[f]	L[g]	T1[h]	T2[h]	β[i]	F_T Mean[j]	Age$_{corr.}$[k]	Error[c]	Calculated
		pmol	1σ	pmol	1σ		fmol/pmol	1σ	Ma	1σ	µm	µm	µm	µm	µm	(1/µm)		Ma	2σ	% ^{4}He loss[l]
Apatites																				
ClUP 08099	a004	0.0860	0.0015	0.2091	0.0035	2.45	0.510	0.016	2.96	0.10	-	39.2	114.6	-	-	0.0763	0.63	**4.69**	**0.31**	93.4
	a008	0.2116	0.0028	0.0623	0.0019	0.30	1.04	0.02	3.58	0.09	-	34.1	127.2	-	-	0.0835	0.61	**5.83**	**0.28**	91.5
	a001	0.1386	0.0023	0.3616	0.0053	2.63	9.24	0.12	32.37	0.56	-	39.8	163.7	-	-	0.0703	0.66	**49.36**	**1.71**	20.0
	a005	0.5148	0.0054	0.2959	0.0048	0.58	31.65	0.38	42.17	0.65	-	43.2	161.8	-	-	0.0658	0.69	**61.51**	**1.90**	-
ClUP 08100	a012	0.1428	0.0069	0.3291	0.0046	2.32	0.104	0.008	0.370	0.032	-	34.0	128.0	-	-	0.0835	0.60	**0.616**	**0.107**	100.1
	a001	0.1047	0.0022	0.3103	0.0086	2.98	0.109	0.012	0.480	0.052	-	31.7	110.7	-	-	0.0909	0.57	**0.845**	**0.183**	99.7
	a014	0.0868	0.0052	0.1145	0.0021	1.33	0.655	0.018	4.50	0.24	-	52.9	102.7	-	-	0.0631	0.69	**6.50**	**0.70**	90.4
	a005	0.0607	0.0025	0.0985	0.0019	1.63	0.416	0.017	3.89	0.20	-	32.5	108.4	-	-	0.1012	0.58	**6.70**	**0.69**	90.1
	a006	0.0362	0.0028	0.0573	0.0027	1.60	0.322	0.013	5.08	0.36	-	31.9	69.8	-	-	0.1012	0.53	**9.51**	**1.35**	85.5
	a008	0.0226	0.0027	0.0123	0.0012	0.548	0.175	0.010	5.36	0.66	-	31.2	80.2	-	-	0.099	0.55	**9.74**	**2.40**	85.1
	a007	0.0788	0.0037	0.1184	0.0038	1.51	2.761	0.045	20.25	0.79	-	33.3	87.1	-	-	0.0923	0.57	**35.57**	**2.78**	42.6
	a002	0.0144	0.0014	0.0457	0.0026	3.21	0.872	0.017	27.2	1.8	-	27.4	100.7	-	-	0.1043	0.51	**52.98**	**6.93**	14.0
Zircons																				
ClUP 08099	z001	10.37	0.12	4.917	0.068	0.478	0.05841	0.00068	3.960	0.061	32.5	32.8	145.6	27.9	28.8	0.0751	0.70	**5.67**	**0.18**	97.5
	z003	7.418	0.075	3.367	0.047	0.457	0.05763	0.00066	5.482	0.081	30.9	33.3	142.4	32.2	29.1	0.0771	0.69	**7.93**	**0.23**	96.3
	z004	8.77	0.10	4.412	0.053	0.507	0.3103	0.0036	24.67	0.39	28.9	31.5	203.9	32.2	37.1	0.0759	0.70	**35.49**	**1.13**	82.3
	z002	28.15	0.27	17.02	0.20	0.609	2.173	0.025	52.60	0.76	34.8	40.6	226.0	43.0	32.9	0.0619	0.75	**70.43**	**2.02**	64.5
	z005	4.314	0.051	2.527	0.034	0.590	0.6214	0.0073	98.1	1.6	26.3	33.8	188.2	31.1	28.2	0.0777	0.69	**142.64**	**4.56**	27.8
ClUP 08100	z003	2.614	0.037	1.628	0.027	0.627	0.001664	0.000029	0.4341	0.0093	29.8	30.5	105.6	24.1	23.7	0.0866	0.66	**0.662**	**0.029**	100.0
	z001	13.47	0.14	7.772	0.096	0.581	0.03041	0.00037	1.553	0.024	28.7	31.7	126.1	20.4	22.7	0.0819	0.67	**2.31**	**0.07**	99.2
	z005	0.793	0.014	0.663	0.017	0.842	0.03081	0.00038	25.36	0.50	26.1	29.9	116.7	34.1	31.0	0.0925	0.63	**40.07**	**1.57**	80.0
	z002	0.975	0.016	0.717	0.017	0.741	0.04675	0.00056	31.87	0.59	23.3	29.3	84.3	19.9	21.0	0.1033	0.60	**53.48**	**1.98**	73.1
	z004	1.943	0.027	0.619	0.016	0.321	0.3300	0.0039	122.1	2.2	27.9	24.8	114.4	33.0	31.3	0.0977	0.62	**197.25**	**6.99**	-

[a] The missing grain numbers represent grains that were determined to contain inclusions, which were not detected during mineral picking. These were identified by the helium re-extraction failing to yield blank levels, which would be the case for inclusion-free apatites.

[b] Absolute concentrations measured for ^{4}He, ^{238}U, and ^{232}Th are used to calculate a "raw age" that does not reflect ^{4}He loss due to a-ejection.

[c] The propagated analytical uncertainty.

[d] ^{4}He yields are in femto-mol for the apatite analyses and in pico-mol for the zircon analyses.

[e] The "raw age" was calculated with an iterative approach to solving the age equation.

[f] R2 values for the apatites are the half-widths of equi-dimensional hexagonal prisms, and R1 and R2 values for the zircons are half-widths for tetragonal prisms.

[g] L represents the total crystal length.

[h] T1 and T2 represent the length of each pyramidal termination in the zircons.

[i] β represents the surface-area-to-volume ratio for the crystals.

[j] The mean F_T (alpha-ejection correction) was calculated assuming a bipyramidal tetragon prism geometry for the zircons (Hourigan et al. 2005), and an equi-dimensional hexagon prism geometry for the apatites (Farley et al., 1996).

[k] A F_T correction was applied to the "raw age" following the procedures of Farley et al. (1996).

[l] % Calculated ^{4}He loss determined using equation [4], assuming the oldest apatite (61.51 Ma) and zircon (197.25 Ma) (U-Th)/He ages (shown by - symbols) and an impact event age of 0.663 Ma.

Table 1

Contact and compression event

Mineral	Grain radius (μm)	Temperature (°C)	Time (seconds)[a]	Modeled % ^{4}He loss[b]	Notes[c]
Apatite	27.4 (min.)	1500	0.000273	60.9	4.91 m impactor (min.)
Apatite	32.9 (av. reset)	1500	0.000273	52.3	4.91 m impactor (min.)
Apatite	52.9 (max.)	1500	0.000273	34.4	4.91 m impactor (min.)
Apatite	27.4 (min.)	1600	0.000273	79.4	4.91 m impactor (min.)
Apatite	32.9 (av. reset)	1600	0.000273	70.0	4.91 m impactor (min.)
Apatite	52.9 (max.)	1600	0.000273	47.6	4.91 m impactor (min.)
Apatite	27.4 (min.)	1500	0.000431	72.4	7.76 m impactor (max.)
Apatite	32.9 (av. reset)	1500	0.000431	81.6	7.76 m impactor (max.)
Apatite	52.9 (max.)	1500	0.000431	42.2	7.76 m impactor (max.)
Apatite	27.4 (min.)	1600	0.000431	89.8	7.76 m impactor (max.)
Apatite	32.9 (av. reset)	1600	0.000431	63.1	7.76 m impactor (max.)
Apatite	52.9 (max.)	1600	0.000431	57.7	7.76 m impactor (max.)
Zircon	24.8 (min.)	1500	0.000273	4.9	4.91 m impactor (min.)
Zircon	30.5 (reset)	1500	0.000273	4.0	4.91 m impactor (min.)
Zircon	40.6 (max.)	1500	0.000273	3.0	4.91 m impactor (min.)
Zircon	24.8 (min.)	1600	0.000273	7.6	4.91 m impactor (min.)
Zircon	30.5 (reset)	1600	0.000273	6.2	4.91 m impactor (min.)
Zircon	40.6 (max.)	1600	0.000273	4.7	4.91 m impactor (min.)
Zircon	24.8 (min.)	1500	0.000431	6.1	7.76 m impactor (max.)
Zircon	30.5 (reset)	1500	0.000431	5.0	7.76 m impactor (max.)
Zircon	40.6 (max.)	1500	0.000431	3.8	7.76 m impactor (max.)
Zircon	24.8 (min.)	1600	0.000431	9.5	7.76 m impactor (max.)
Zircon	30.5 (reset)	1600	0.000431	7.7	7.76 m impactor (max.)
Zircon	40.6 (max.)	1600	0.000431	5.8	7.76 m impactor (max.)

Adiabatic decompression and shock metamorphism event

Mineral	Grain radius (μm)	Temperature (°C)	Time (seconds)	Modeled % ^{4}He loss[b]
Apatite	27.4 (min.)	1,500	1 (max.)	100.0
Apatite	27.4 (min.)	1,500	0.1 (min.)	100.0
Apatite	27.4 (min.)	1,600	1 (max.)	100.0
Apatite	27.4 (min.)	1,600	0.1 (min.)	100.0
Apatite	32.9 (av. reset)	1,500	1 (max.)	100.0
Apatite	32.9 (av. reset)	1,500	0.1 (min.)	100.0
Apatite	32.9 (av. reset)	1,600	1 (max.)	100.0
Apatite	32.9 (av. reset)	1,600	0.1 (min.)	100.0
Apatite	52.9 (max.)	1,500	1 (max.)	100.0
Apatite	52.9 (max.)	1,500	0.1 (min.)	100.0
Apatite	52.9 (max.)	1,600	1 (max.)	100.0
Apatite	52.9 (max.)	1,600	0.1 (min.)	100.0
Zircon	24.8 (min.)	1,500	1 (max.)	71.2
Zircon	24.8 (min.)	1,500	0.1 (min.)	100.0
Zircon	24.8 (min.)	1,600	1 (max.)	90.8
Zircon	24.8 (min.)	1,600	0.1 (min.)	100.0
Zircon	30.5 (av.)	1,500	1 (max.)	61.5
Zircon	30.5 (av.)	1,500	0.1 (min.)	99.6
Zircon	30.5 (av.)	1,600	1 (max.)	82.5
Zircon	30.5 (av.)	1,600	0.1 (min.)	100.0
Zircon	40.6 (max.)	1,500	1 (max.)	49.1
Zircon	40.6 (max.)	1,500	0.1 (min.)	96.6
Zircon	40.6 (max.)	1,600	1 (max.)	69.0
Zircon	40.6 (max.)	1,600	0.1 (min.)	99.9

Abbreviations: min. = minimum, av. = average, max. = maximum, E = activation energy, and D_o = frequency factor.

[a] Time (seconds) calculated using equation [1].

[b] Modeled % ^{4}He loss calculated using equations [2-3], using the following He diffusion parameters: apatite (E = 32.9 kcal/mol, D_o = 31.62 cm^2/s with cylindrical diffusion geometry; Farley, 2000), and zircon (E = 40.4 kcal/mol, D_o = 0.45 cm^2/s with spherical diffusion geometry; Reiners et al., 2004).

[c] Impact size calculated using *Crater* (Melosh and Beyer, 2002) and *Impact and Explosion Effects* (Holsapple, 2020) online software.

Table 2

Table 1: (U-Th)/He geochronolgical analyses of apatites and zircons from the Monturaqui impact crater

Sample	Grain#[a]	[^{238}U][b]	Error[c]	[^{232}Th][b]	Error[c]	Th/U	[^{4}He][b,d]	Error[c]	Age$_{raw}$[e]	Error[c]	R1[f]	R2[f]	L[g]	T1[h]	T2[h]	β[i]	F_T Mean[j]	Age$_{corr.}$[k]	Error[c]	Calculated
		pmol	1σ	pmol	1σ		fmol/pmol	1σ	Ma	1σ	μm	μm	μm	μm	μm	(1/μm)		Ma	2σ	% ^{4}He loss[l]
Apatites																				
CIUP 08099	a004	0.0860	0.0015	0.2091	0.0035	2.45	0.510	0.016	2.96	0.10	-	39.2	114.6	-	-	0.0763	0.63	**4.69**	**0.31**	93.4
	a008	0.2116	0.0028	0.0623	0.0019	0.30	1.04	0.02	3.58	0.09	-	34.1	127.2	-	-	0.0835	0.61	**5.83**	**0.28**	91.5
	a001	0.1386	0.0023	0.3616	0.0053	2.63	9.24	0.12	32.37	0.56	-	39.8	163.7	-	-	0.0703	0.66	**49.36**	**1.71**	20.0
	a005	0.5148	0.0054	0.2959	0.0048	0.58	31.65	0.38	42.17	0.65	-	43.2	161.8	-	-	0.0658	0.69	**61.51**	**1.90**	-
CIUP 08100	a012	0.1428	0.0069	0.3291	0.0046	2.32	0.104	0.008	0.370	0.032	-	34.0	128.0	-	-	0.0835	0.60	**0.616**	**0.107**	100.1
	a001	0.1047	0.0022	0.3103	0.0086	2.98	0.109	0.012	0.480	0.052	-	31.7	110.7	-	-	0.0909	0.57	**0.845**	**0.183**	99.7
	a014	0.0868	0.0052	0.1145	0.0021	1.33	0.655	0.018	4.50	0.24	-	52.9	102.7	-	-	0.0631	0.69	**6.50**	**0.70**	90.4
	a005	0.0607	0.0025	0.0985	0.0019	1.63	0.416	0.017	3.89	0.20	-	32.5	108.4	-	-	0.1012	0.58	**6.70**	**0.69**	90.1
	a006	0.0362	0.0028	0.0573	0.0027	1.60	0.322	0.013	5.08	0.36	-	31.9	69.8	-	-	0.1012	0.53	**9.51**	**1.35**	85.5
	a008	0.0226	0.0027	0.0123	0.0012	0.548	0.175	0.010	5.36	0.66	-	31.2	80.2	-	-	0.099	0.55	**9.74**	**2.40**	85.1
	a007	0.0788	0.0037	0.1184	0.0038	1.51	2.761	0.045	20.25	0.79	-	33.3	87.1	-	-	0.0923	0.57	**35.57**	**2.78**	42.6
	a002	0.0144	0.0014	0.0457	0.0026	3.21	0.872	0.017	27.2	1.8	-	27.4	100.7	-	-	0.1043	0.51	**52.98**	**6.93**	14.0
Zircons																				
CIUP 08099	z001	10.37	0.12	4.917	0.068	0.478	0.05841	0.00068	3.960	0.061	32.5	32.8	145.6	27.9	28.8	0.0751	0.70	**5.67**	**0.18**	97.5
	z003	7.418	0.075	3.367	0.047	0.457	0.05763	0.00066	5.482	0.081	30.9	33.3	142.4	32.2	29.1	0.0771	0.69	**7.93**	**0.23**	96.3
	z004	8.77	0.10	4.412	0.053	0.507	0.3103	0.0036	24.67	0.39	28.9	31.5	203.9	32.2	37.1	0.0759	0.70	**35.49**	**1.13**	82.3
	z002	28.15	0.27	17.02	0.20	0.609	2.173	0.025	52.60	0.76	34.8	40.6	226.0	43.0	32.9	0.0619	0.75	**70.43**	**2.02**	64.5
	z005	4.314	0.051	2.527	0.034	0.590	0.6214	0.0073	98.1	1.6	26.3	33.8	188.2	31.1	28.2	0.0777	0.69	**142.64**	**4.56**	27.8
CIUP 08100	z003	2.614	0.037	1.628	0.027	0.627	0.001664	0.000029	0.4341	0.0093	29.8	30.5	105.6	24.1	23.7	0.0866	0.66	**0.662**	**0.029**	100.0
	z001	13.47	0.14	7.772	0.096	0.581	0.03041	0.00037	1.553	0.024	28.7	31.7	126.1	20.4	22.7	0.0819	0.67	**2.31**	**0.07**	99.2
	z005	0.793	0.014	0.663	0.017	0.842	0.03081	0.00038	25.36	0.50	26.1	29.9	116.7	34.1	31.0	0.0925	0.63	**40.07**	**1.57**	80.0
	z002	0.975	0.016	0.717	0.017	0.741	0.04675	0.00056	31.87	0.59	23.3	29.3	84.3	19.9	21.0	0.1033	0.60	**53.48**	**1.98**	73.1
	z004	1.943	0.027	0.619	0.016	0.321	0.3300	0.0039	122.1	2.2	27.9	24.8	114.4	33.0	31.3	0.0977	0.62	**197.25**	**6.99**	-

[a] The missing grain numbers represent grains that were determined to contain inclusions, which were not detected during mineral picking. These were identified by the helium re-extraction failing to yield blank levels, which would be the case for inclusion-free apatites.

[b] Absolute concentrations measured for ^{4}He, ^{238}U, and ^{232}Th are used to calculate a "raw age" that does not reflect ^{4}He loss due to a-ejection.

[c] The propagated analytical uncertainty.

[d] ^{4}He yields are in femto-mol for the apatite analyses and in pico-mol for the zircon analyses.

[e] The “raw age” was calculated with an iterative approach to solving the age equation.

[f] R2 values for the apatites are the half-widths of equi-dimensional hexagonal prisms, and R1 and R2 values for the zircons are half-widths for tetragonal prisms.

[g] L represents the total crystal length.

[h] T1 and T2 represent the length of each pyramidal termination in the zircons.

[i] β represents the surface-area-to-volume ratio for the crystals.

[j] The mean F_T (alpha-ejection correction) was calculated assuming a bipyramidal tetragon prism geometry for the zircons (Hourigan et al. 2005), and an equi-dimensional hexagon prism geometry for the apatites (Farley et al., 1996).

[k] A F_T correction was applied to the “raw age” following the procedures of Farley et al. (1996).

[l] % Calculated ^{4}He loss determined using equation [4], assuming the oldest apatite (61.51 Ma) and zircon (197.25 Ma) (U-Th)/He ages (shown by - symbols) and an impact event age of 0.663 Ma.

Table 2. Modeling of ^{4}He loss from apatite and zircon grains during Monturaqui impact crater-forming stages.

Contact and compression event

Mineral	Grain radius (μm)	Temperature (°C)	Time (seconds)[a]	Modeled % ^{4}He loss[b]	Notes[c]
Apatite	27.4 (min.)	1500	0.000273	60.9	4.91 m impactor (min.)
Apatite	32.9 (av. reset)	1500	0.000273	52.3	4.91 m impactor (min.)
Apatite	52.9 (max.)	1500	0.000273	34.4	4.91 m impactor (min.)
Apatite	27.4 (min.)	1600	0.000273	79.4	4.91 m impactor (min.)
Apatite	32.9 (av. reset)	1600	0.000273	70.0	4.91 m impactor (min.)
Apatite	52.9 (max.)	1600	0.000273	47.6	4.91 m impactor (min.)
Apatite	27.4 (min.)	1500	0.000431	72.4	7.76 m impactor (max.)
Apatite	32.9 (av. reset)	1500	0.000431	81.6	7.76 m impactor (max.)
Apatite	52.9 (max.)	1500	0.000431	42.2	7.76 m impactor (max.)
Apatite	27.4 (min.)	1600	0.000431	89.8	7.76 m impactor (max.)
Apatite	32.9 (av. reset)	1600	0.000431	63.1	7.76 m impactor (max.)
Apatite	52.9 (max.)	1600	0.000431	57.7	7.76 m impactor (max.)
Zircon	24.8 (min.)	1500	0.000273	4.9	4.91 m impactor (min.)
Zircon	30.5 (reset)	1500	0.000273	4.0	4.91 m impactor (min.)
Zircon	40.6 (max.)	1500	0.000273	3.0	4.91 m impactor (min.)
Zircon	24.8 (min.)	1600	0.000273	7.6	4.91 m impactor (min.)
Zircon	30.5 (reset)	1600	0.000273	6.2	4.91 m impactor (min.)
Zircon	40.6 (max.)	1600	0.000273	4.7	4.91 m impactor (min.)
Zircon	24.8 (min.)	1500	0.000431	6.1	7.76 m impactor (max.)
Zircon	30.5 (reset)	1500	0.000431	5.0	7.76 m impactor (max.)
Zircon	40.6 (max.)	1500	0.000431	3.8	7.76 m impactor (max.)
Zircon	24.8 (min.)	1600	0.000431	9.5	7.76 m impactor (max.)
Zircon	30.5 (reset)	1600	0.000431	7.7	7.76 m impactor (max.)
Zircon	40.6 (max.)	1600	0.000431	5.8	7.76 m impactor (max.)

Adiabatic decompression and shock metamorphism event

Mineral	Grain radius (μm)	Temperature (°C)	Time (seconds)	Modeled % ^{4}He loss[b]
Apatite	27.4 (min.)	1,500	1 (max.)	100.0
Apatite	27.4 (min.)	1,500	0.1 (min.)	100.0
Apatite	27.4 (min.)	1,600	1 (max.)	100.0
Apatite	27.4 (min.)	1,600	0.1 (min.)	100.0
Apatite	32.9 (av. reset)	1,500	1 (max.)	100.0
Apatite	32.9 (av. reset)	1,500	0.1 (min.)	100.0
Apatite	32.9 (av. reset)	1,600	1 (max.)	100.0
Apatite	32.9 (av. reset)	1,600	0.1 (min.)	100.0
Apatite	52.9 (max.)	1,500	1 (max.)	100.0
Apatite	52.9 (max.)	1,500	0.1 (min.)	100.0
Apatite	52.9 (max.)	1,600	1 (max.)	100.0
Apatite	52.9 (max.)	1,600	0.1 (min.)	100.0
Zircon	24.8 (min.)	1,500	1 (max.)	71.2
Zircon	24.8 (min.)	1,500	0.1 (min.)	100.0
Zircon	24.8 (min.)	1,600	1 (max.)	90.8
Zircon	24.8 (min.)	1,600	0.1 (min.)	100.0
Zircon	30.5 (av.)	1,500	1 (max.)	61.5
Zircon	30.5 (av.)	1,500	0.1 (min.)	99.6
Zircon	30.5 (av.)	1,600	1 (max.)	82.5
Zircon	30.5 (av.)	1,600	0.1 (min.)	100.0
Zircon	40.6 (max.)	1,500	1 (max.)	49.1
Zircon	40.6 (max.)	1,500	0.1 (min.)	96.6
Zircon	40.6 (max.)	1,600	1 (max.)	69.0
Zircon	40.6 (max.)	1,600	0.1 (min.)	99.9

Abbreviations: min. = minimum, av. = average, max. = maximum, E = activation energy, and D_o = frequency factor.

[a] Time (seconds) calculated using equation [1].

[b] Modeled % ^{4}He loss calculated using equations [2-3], using the following He diffusion parameters: apatite (E = 32.9 kcal/mol, D_o = 31.62 cm^2/s with cylindrical diffusion geometry; Farley, 2000), and zircon (E = 40.4 kcal/mol, D_o = 0.45 cm^2/s with spherical diffusion geometry; Reiners et al., 2004).

[c] Impact size calculated using *Crater* (Melosh and Beyer, 2002) and *Impact and Explosion Effects* (Holsapple, 2020) online software.

Declaration of interests

☒ The authors declare that they have no known competing financial interests or personal relationships that could have appeared to influence the work reported in this paper.

☐The authors declare the following financial interests/personal relationships which may be considered as potential competing interests: